Newton

CellPress
OPEN ACCESS

Review

Recent advances in high-dimensional quantum frequency combs

Kai-Chi Chang,[1,2,3,*] Xiang Cheng,[1,2,3,*] Murat Can Sarihan,[1,2] and Chee Wei Wong[1,2,*]
[1]Fang Lu Mesoscopic Optics and Quantum Electronics Laboratory, Department of Electrical and Computer Engineering, University of California, Los Angeles, Los Angeles, CA 90095, USA
[2]Center for Quantum Science and Engineering, University of California, Los Angeles, Los Angeles, CA 90095, USA
[3]These authors contributed equally
*Correspondence: uclakcchang@ucla.edu (K.-C.C.), chengxiang@ucla.edu (X.C.), cheewei.wong@ucla.edu (C.W.W.)
https://doi.org/10.1016/j.newton.2025.100024

ACCESSIBLE OVERVIEW Quantum frequency combs are specialized quantum light sources that emit light of multiple, evenly spaced frequencies. They are powerful tools that can enable multiple information channels across time and frequency domains, all within a single spatial optical mode. This unique ability makes them ideal for creating and controlling high-dimensional entanglement in complex quantum states. High-dimensional quantum systems, or qudits, are key to advancing quantum technologies because they can store and process denser information than traditional binary quantum systems, or qubits. These qudit systems are valuable for fundamental research and applications such as quantum information processing, quantum secure communication, efficient quantum computing, and quantum metrology. This article reviews recent advancements in high-dimensional quantum frequency comb technology, highlighting its ability to generate and control advanced states using commercially available telecom photonic components. These breakthroughs are driving the development of large-scale, practical quantum systems and unlocking new possibilities in future quantum science and technology.

SUMMARY

High-dimensional entanglement in qudit states offers a promising pathway toward the realization of practical, large-scale quantum systems that are highly controllable. These systems can be leveraged for various applications, including advanced quantum information processing, secure communications, computation, and metrology. In this context, quantum frequency combs have a crucial role as they inherently support multiple modes in both temporal and frequency domains, while preserving a single spatial mode. The multiple temporal and frequency modes of quantum frequency combs facilitate the generation, characterization, and control of high-dimensional time-frequency entanglement in extensive quantum systems. In this review article, we provide an overview of recent technological advancements in high-dimensional energy-time entangled quantum frequency combs. We explore how these time-frequency qudits, achieved using scalable telecommunications-wavelength components, can empower the creation of large-scale quantum states. Advances in quantum frequency combs can unlock new capabilities and versatility for promising developments in quantum science and technology.

INTRODUCTION

The qubit, a fundamental unit in quantum information processing, is a two-dimensional or two-state system. A qudit, representing a quantum system with d dimensions, introduces a higher level of complexity due to the scaling of the Hilbert space dimensionality with d^N (where d and N denote the number of dimensions and particles, respectively). This increased dimensionality aids the generation of large-scale quantum systems, serving as a foundation for essential tests of nature that aim to address fundamental loopholes[1–4] as well as practical quantum applications. The high-dimensional quantum states offer significant advantages, including a substantial boost in quantum information capacity, enhanced link speeds,[5–10] improved resilience to noise in quantum communications,[6,10–14] advanced capabilities in quantum metrology,[15,16] and the facilitation of novel algorithms for quantum simulations and computations.[17–20]

Various physical platforms offer unique capabilities for encoding and decoding large-scale quantum states, including atomic systems,[21] superconducting devices,[22] and photonic qudits.[23]

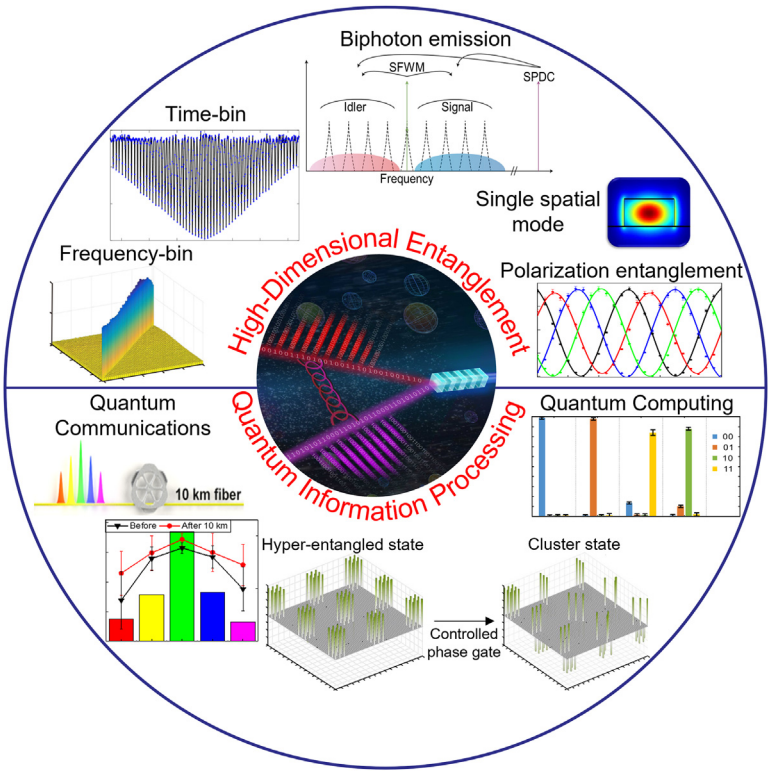

Figure 1. Properties and applications of high-dimensional QFCs

Mode-locked QFCs feature the biphoton emission, combined DoFs in a single spatial mode, and a variety of high-dimensional entangled states can be generated to pioneer emerging research fields. The middle inset figure was generated by Nicoletta Barolini.

In general, photonic systems excel in quantum communication, atomic systems offer stability and long coherence, while superconducting devices provide advantages in quantum computations. Here, we focus on the quantum photonic systems. In photonic qudit platforms, two fundamentally distinct methods are used to harness quantum information: continuous-variable and discrete-variable methods. The continuous-variable approach involves manipulating quantum information via the quantized electric field quadrature of squeezed states,[24,25] while the discrete-variable approach utilizes Fock states.[26–28]

Continuous-variable systems encode quantum states in the continuous amplitude and phase of photons across different degrees of freedom (DoFs) and platforms.[29] Recently, time and frequency variables have also been proposed as quantum continuous variables, offering advantages for quantum information processing in the continuous-variable framework.[30] The main advantage of continuous-variable systems is the deterministic generation and room temperature detection using homodyne photodiodes. However, existing systems usually rely on optical parametric oscillators (OPOs), which are often bulky and require sophisticated stabilization.[31–40] To address this, continuous-variable squeezed quantum frequency combs (QFCs) have recently been demonstrated using on-chip platforms.[41–45]

Discrete-variable systems, on the other hand, create and detect different DoFs of single photons, allowing for the generation and precise control of individual modes in large-scale integrated quantum systems.[46–49] The main advantage of discrete-variable systems is their ability to realize entangled states with near-unity fidelity and precise control over individual modes. However, current technology mainly relies on probabilistic entangled sources, posing scalability challenges as the number of qudits (N) increases. To overcome this, incorporating deterministic high-fidelity single-photon sources,[50,51] state-of-the-art superconducting nanowire single-photon detectors (SNSPDs) with near-unity detection efficiency,[52–54] ultra-low dark counts,[55] and minimal timing jitters[56] is essential. These advancements aim to achieve deterministic, unit-fidelity quantum information processing with single photons.

The initial creation and control of discrete-variable high-dimensional photonic systems have been successful in manipulating quantum information in spatial and orbital angular momentum modes.[57–75] However, the footprint and complexity of these approaches increase with the number of dimensions (d) or particles (N) of the qudit, primarily due to the spatial nature of the utilized DoFs, limiting the attainable complexity for practical systems.

In stark contrast, there has been a rapid investigation into the discretized temporal and spectral modes of mode-locked QFCs.[76,77] This trend marks a departure from previous approaches and has gained significant attention in recent studies.[78–100] These recent studies enable the coherent generation, characterization, and control of high-dimensional,[80,81,83,100] hyperentangled,[80,89,101,102] or multipartite states[87,89] in a single spatial mode. In particular, the first high-dimensional QFCs appeared in Xie et al.[80] Then, the generation and control of multi-dimensional QFCs in telecommunication integrated systems was achieved in Reimer and co-workers.[81,83] Later, high-dimensional QFCs have been utilized for quantum computational processing.[87,89] The multimode temporal and spectral properties of mode-locked QFCs provide a unique opportunity for dense quantum information processing, making them well suited for practical applications involving high-dimensional hyperentangled quantum systems.

Here, we review recent progress on the realization and applications of high-dimensional energy-time entangled mode-locked QFCs (see Figure 1). Previous reviews have covered continuous-variable quantum information processing using squeezed states,[25,26,30] and demonstrations utilizing other discrete-variable DoFs of entangled photons for complex quantum information processing and using integrated chips.[103–108] This review addresses the generation, characterization, and control of high-dimensional QFCs in the time and frequency domains, focusing on QFCs generated in nonlinear optical

waveguides via post-filtering cavities and with cavity enhancement, and QFCs generated from on-chip microresonators. Finally, we explore the potential of these *d*-level QFCs for future large-scale photonic quantum science and technology applications.

GENERATION MECHANISM OF MODE-LOCKED QFCs

In this section, we focus on generating, characterizing, and control of discrete temporal and spectral modes within high-dimensional QFCs. We discuss methods for creating qudit states, techniques for their characterization, and strategies for their control. We particularly focus on the local and non-local measurements in QFCs with biphotons, which are of interest from both fundamental and application perspectives.

Most configurations for creating entangled photon pairs in two or higher dimensions rely on the inherently probabilistic photon-pair generation processes, such as spontaneous parametric downconversion (SPDC) and spontaneous four-wave mixing. SPDC uses a $\chi^{(2)}$ nonlinearity to convert a higher-energy pump photon into two lower-energy photons (signal and idler) through three-wave mixing. Spontaneous four-wave mixing, on the other hand, is a third-order nonlinear effect where signal and idler photons are generated by the annihilation of two pump photons.

Mode-locked QFCs exhibit discrete spectral and temporal modes, and can be generated via SPDC photons with post-filtering, cavity enhancement, or spontaneous four-wave mixing in a microresonator.[108] In the time domain, the wavefunction of a QFC state is expressed as:

$$|\psi\rangle = \int d\tau e^{-\Delta\omega|\tau|} \sum_{m=-N_0}^{N_0} \mathrm{sinc}(Am\Delta\Omega)\cos(m\Delta\Omega\tau)\hat{a}_H^\dagger(t)\hat{a}_V^\dagger(t+\tau)|0\rangle, \quad \text{(Equation 1)}$$

where the sinc function is the SPDC's phase-matching function with A related to the phase-matching bandwidth, $\hat{a}_H^\dagger$ and $\hat{a}_V^\dagger$ are creation operators for horizontally and vertically polarized photons, $\Delta\Omega$ is the cavity FSR in rad s^{-1}, Ω is the detuning of the SPDC's biphotons from frequency degeneracy, $2N_0 + 1$ is the number of cavity lines passed by an overall bandwidth-limiting filter, $\Delta\omega$ is the half of FWHM linewidth of cavity's Lorentzian transmission lineshape, τ is the relative time delay between signal and idler photons.

The mode-locking mechanism, a well-established technique in ultrafast optics,[109] is crucial for generating mode-locked QFCs. It is important to note the distinction in the term mode locking between mode-locked laser pulses, classical frequency combs, and mode-locked QFCs[108]—in the classical domain, phase coherence among all mode-locked modes is essential to generate ultrafast pulses and classical frequency combs, whereas in the quantum regime, mode locking refers primarily to phase stability between two photons in a QFC.

In 1999, Ou and Lu observed the first quantum mode-locked biphoton state in a cavity-enhanced SPDC source using a Fabry-Perot cavity[76] (Figure 2A). The cavity was formed with the end facets of the nonlinear crystal as one reflecting surface. By filtering out non-degenerate pairs with a passive filter cavity, they measured the single-frequency-mode temporal distribution of biphotons and extracted a cavity bandwidth of 44 MHz (Figure 2B). A few years later, the same group created another mode-locked two-photon state (Figure 2C) using a fiber cavity to filter SPDC photons, discretizing their spectrum.[77] They observed the mode-locking process by measuring the first Hong-Ou-Mandel (HOM) revivals (Figure 2D), as predicted by Shapiro,[110] noting that the HOM revival period was half the cavity round-trip time. In mode-locked QFC generation, biphotons with either a delay of one cavity round-trip time or simultaneous occurrence show coherence, both producing HOM interference.[77] Intuitively, from the quantum optics perspective, HOM interference reveals the time-frequency indistinguishability of photon pairs generated in a multimode QFC. Therefore, HOM interference probes local indistinguishability and the multimode structure of QFCs, revealing how the modes are correlated in the time-frequency domain. In 2015, researchers observed high-visibility HOM revival interferences (central HOM dip visibility up to 96.5% after accidental subtractions) with 19 HOM dips, expanding usable temporal modes in QFCs[80] (Figure 2E). More recently, high-visibility HOM revival interferences were measured in a cavity-enhanced mode-locked biphoton state over a large path length difference.[111] Using a 100 GHz phase-matching bandwidth SPDC crystal, a 120.8 MHz FSR bow-tie cavity, and optical fiber with delays of multiple cavity round-trip times, they demonstrated HOM interferences up to the 84th dip, corresponding to a 105-m pathlength difference (Figure 2F).

Besides the QFC generation scheme using SPDC photons in cavities, recently, integrated QFC with spontaneous four-wave mixing has also become a rapidly growing field of research.[81–85] Similar to the QFC generation scheme in Figure 2A, integrated QFC from spontaneous four-wave mixing is also a cavity-enhanced process. The phase-matching condition in spontaneous four-wave mixing is typically designed such that the bandwidth of the photon pair can cover multiple resonances, which occurs under low anomalous second-order dispersion.[78,81,83] What makes integrated QFCs particularly attractive is that they intrinsically support multiple temporal and spectral modes in an on-chip device, providing advantages of miniaturization and low power consumption. Integrated QFCs were first observed in OPOs pumped below threshold.[78,79] Due to their small footprint, these multimodal sources support cavity FSR in the range of a few dozens to a few hundreds of GHz, which is well suited for commercial telecom technologies.[81–85] In addition to cavity-based QFC generation, QFC-like structures can be generated by using quantum interference to modulate the continuous spectrum of photon pairs to generate a QFC-like structure[112,113] or by using domain-engineered phase-matching conditions in the SPDC process.[114,115]

To fully utilize the multimode structure in QFCs, it is essential to measure and characterize the temporal and spectral properties of entangled photon pairs. The frequency spectrum of QFCs shows a multimode feature while conserving energy and momentum in the SPDC process, leading to discretized anti-correlation in the joint spectral intensity (JSI). Due to Fourier transform duality, QFCs generate a strong multimode temporal correlation in the joint temporal intensity (JTI) when signal and idler photons are created simultaneously within the biphoton's coherence

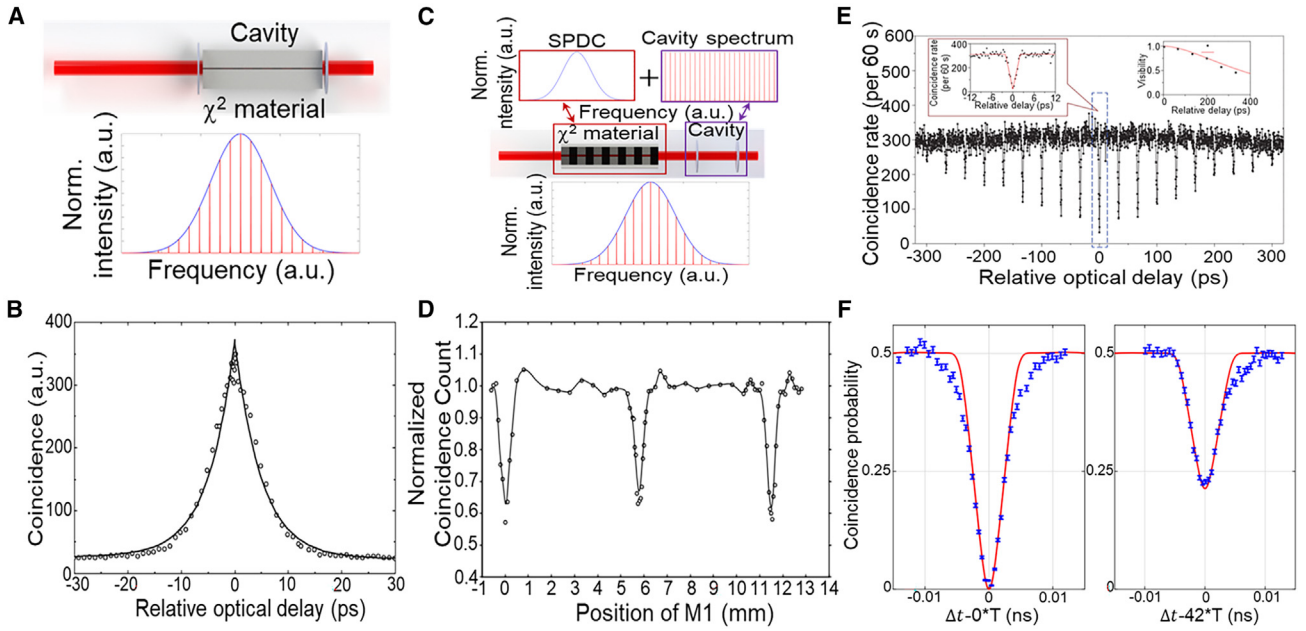

Figure 2. Cavity mode-locked mechanism and recurrences of second-order signatures in QFCs

(A) The schematic for the generation of mode-locked two-photon states in a Fabry-Perot-type cavity-enhanced SPDC.

(B) Temporal correlation signatures of single-frequency-mode two-photon states in a cavity-enhanced SPDC.

(C) Principles of mode-locked QFC generation using post-filtered SPDC entangled photon pairs. Example SPDC and cavity spectrum and the output of post-filtered QFC spectrum. The dark red arrow and box are the SPDC spectrum, while the purple arrow and box indicate the spectrum of the filtering cavity. This approach leads to a discrete energy-time correlated QFC. The generated photon pair is entangled across the frequency-bins in the SPDC bandwidth.

(D) The first HOM revival measurements of the mode-locked two-photon states. M1 is the mirror used in the measurement.

(E) The observed high-visibility 19 HOM revival interferences without post-selection in a mode-locked doubly filtered QFC.

(F) Example HOM revival interferences from a cavity-enhanced SPDC source for 0 and 42 round trips. Δt is the coarse time delay, and the T is the cavity round-trip time. In both (E) and (F), the period of HOM revival measurements is half of the cavity round-trip time of the QFCs, resulting from the mode-locking nature of the process. The graphs in (B) are reprinted with permission from Qu and Lu,[76] APS. (D) Reprinted with permission from Lu et al.,[77] APS. (E) Adapted with permission from Xie et al.,[80] Springer Nature Limited. (F) Adapted with permission from Rambach et al.,[111] APS.

time. We next discuss techniques for characterizing the JTI of SPDC two-photon states.

CHARACTERIZING THE JTI OF SPDC

Directly measuring JTI, which represents the probability of detecting biphotons at specific arrival times, is challenging with current SNSPDs due to the femtosecond timescales of SPDC photon correlations. Temporal cross-correlation measurements are feasible only when the timing jitter of detectors (typically 20–200 ps) is smaller than the Fourier transform of the cavity's free spectral range (FSR) for cavity-enhanced SPDC sources with few GHz FSR[116] (Figure 3A) or the Fourier transform bandwidth of SPDC biphotons in narrow phase-matching bandwidth sources.[117] This method provides the most direct measurements for probing the JTI of SPDC photons, and the main limitation is the Fourier transform bandwidth of the photon-pair source or the cavity FSR of QFCs needs to be less than the effective timing resolution of SNSPDs. Alternative methods to bypass this timescale limitation include sum-frequency generation (SFG)-based ultrafast coincidence counting[118–120] (Figure 3B) and temporal magnification with a time lens[121] (Figure 3C). Higher-resolution measurements are possible by the use of SFG-based ultrafast coincidence counting and temporal magnification with a time lens. The former not only enables the JTI to be measured at femtosecond timescales, but also allows for nonlocal dispersion cancellation to be observed at the same timescales. The latter works by magnifying the temporal correlation of biphotons so that even commercial single-photon detectors are able to resolve their JTI. Both methods, however, are complicated to implement. Two-photon interferometry can reconstruct the temporal wavefunction of biphotons[122–126] and, recently, conjugate Franson interferometry has been used to measure the JTI and spectral phase of SPDC photons[127,128] (Figure 3D). This technique provides the JTI measurement of photon pairs by using the interference visibility of conjugate Franson interferometry, since the fringe visibility is sensitive to the spectral phase of biphotons. The main benefit of this method is that it works with commercial single-photon detectors and does not require complicated setups. Yet, the stability and the quality of the interference visibility needs to be stable and high enough for characterizing the JTI of biphotons precisely.

Generally, it can be seen that JTI measurements are limited by the temporal resolution of single-photon detectors, and the Fourier transform bandwidth of the photon pairs. Besides JTI, direct measurement of the joint temporal amplitude (JTA) can

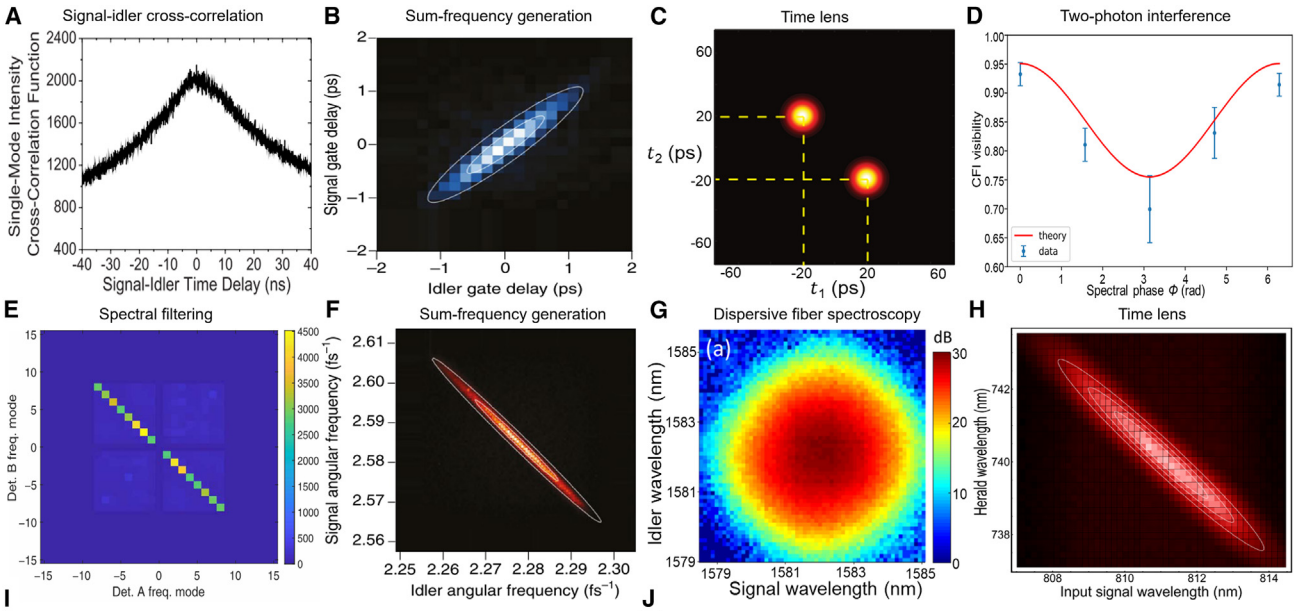

I

Techniques for JTI characterization in SPDC photons	Advantage	Disadvantage
Temporal cross-correlation measurements	Most direct measurements in coincidence counting	The Fourier-transform bandwidth of SPDC photons need to be less than the effective timing resolution of single-photon detectors
Sum-frequency generation (SFG)	Ultrafast coincidence counting with femtosecond time scales	Complicated setup and optical loss
Time lens	Magnifying the temporal correlation of biphotons so that commercial single-photon detectors can do used	Complicated setup and optical loss
Conjugate Franson interferometry (CFI)	Use the interference fringe visibility for the measurement, and it works with commercial single-photon detectors	The stability and the quality of the interference visibility needs to be stable and high enough for precise measurements

J

Techniques for JSI characterization in SPDC photons	Advantage	Disadvantage
Frequency-bin filtering measurements	Most direct measurements in coincidence counting	Bandwidth limitation of few GHz to 100 GHz in telecom wavelengths
Sum-frequency generation (SFG)	Ultrafast coincidence counting with femtosecond time scales	Involved experimental setup and optical loss
Dispersive fiber spectroscopy	Compact measurement setup with less stringent requirements on optical alignment	Spectral resolution is limited by the dispersion of the system and the timing resolution of the single-photon detectors
Time lens	Frequency-resolved single-photon detection with commercial single-photon detectors	Complicated setup and optical loss

Figure 3. Probing joint temporal and spectral characteristics in frequency-correlated SPDC entangled photons

(A) Temporal second-order cross-correlation function between signal and idler photons in a cavity-enhanced SPDC source.

(B) Direct observation of the SPDC JTI with strong positive correlations by using sum-frequency generation (SFG) and ultrafast optical temporal gating pulses.

(C) Measured JTI of SPDC photons with the time lens, showing bunched behavior of biphotons. Here, t_1, t_2 are the time delay for signal and idler photons, respectively.

(D) Two-photon conjugate Franson interference visibility versus a function of applied spectral phase, which can be used to probe the JTI between SPDC photons with the same JSI. Error bars represent one standard deviation of three measurements.

(E) A measurement of the JSI for an eight-dimensional QFC.

(F) Direct measurement of JSI of energy-time entangled SPDC photons using SFG that operates on ultrafast timescales.

(G) Measured JSI profile of SPDC biphotons using dispersive fiber spectroscopy.

(H) Measured JSI of SPDC photons via time lens, with strong frequency anti-correlations.

(I and J) The summary comparison tables for various techniques in JTI and JSI measurements of SPDC photons, respectively. The graph in (A) is reprinted with permission from Shapiro, [110] AIP. (B) Adapted with permission from MacLean et al.,[120] APS. (C) Reprinted from Mittal et al.,[121] APS. (D) Adapted with permission from Chen et al.,[128] APS. (E) Reprinted from Imany et al.,[95] AAAS. (F) Reprinted from MacLean et al.,[120] APS. (G) Adapted with permission from Chen et al.,[129] OSA. (H) Reprinted from Donohue et al.,[130] APS.

provide phase information, but standard coincidence counting lacks tools for full spectral phase probing. JTA can be reconstructed via interferometric techniques[124,126] or temporal amplitude-phase modulation with frequency-resolved detection.[131]

CHARACTERIZING THE JSI OF SPDC

The JSI, the conjugate of JTI, represents the frequency correlation of energy-matched photon pairs and can be measured via spectrally resolved coincidence measurements with standard single-photon detectors.[132] Common methods to characterize the JSI of SPDC biphoton pairs include frequency-bin filtering measurements[99,100,133] (Figure 3E), SFG-based ultrafast coincidence counting[120,134–136] (Figure 3F), dispersive fiber spectroscopy[129,137–144] (Figure 3G), and spectral negative magnification via time lens[121,130] (Figure 3H). The frequency-bin filtering measurements are the most direct method, albeit with the typical bandwidth limitation of a few GHz to 100 GHz in telecom

wavelengths. As was the case for JTI measurements, SFG-based ultrafast coincidence counting and time lenses provide frequency-resolved detection, but at the expense of more involved experimental setups. In contrast, dispersive fiber spectroscopy can be performed in a compact setup with less-stringent requirements on optical alignment, but its spectral resolution is set by the dispersion of the system and the timing resolution of the single-photon detectors. Besides, it is also possible to probe the JSI of SPDC photon pairs by shifting biphoton frequencies by pump tuning or nonlinear crystal control.[145] Finally, in Figures 3I and 3J, we provide summary comparison tables of different techniques used in JTI and JSI measurements of SPDC photons, respectively.

Generally, it can be seen that JSI measurements are limited by the spectral resolution of the various techniques, and the bandwidth of the photon pairs. Similar to JTI measurements, full quantum-state reconstruction with coincidence counting methods is challenging, but direct measurement of joint spectral amplitude (JSA) has been demonstrated,[124,146–148] and new methods such as modified Franson interferometry aim to retrieve full spectral amplitude and phase information.[149] Recently, a dispersion-engineered JSI SPDC source with a record-high 100 THz bandwidth has been demonstrated,[150] and non-phase-matched SPDC sources offer a route to significantly increase the degree of frequency entanglement, surpassing standard phase-matched sources.[151]

In addition to individual characterization of JTI and JSI, Franson and conjugate Franson interferometry can be used together to exploit temporal correlation and spectral anti-correlation,[127,152] enabling phase-sensitive quantum interference in Franson-type interferometers. Franson interferometry uses unbalanced Mach-Zehnder interferometers (MZIs) with a path-length difference (ΔT). To avoid local interference and accurately register indistinguishable single photons, ΔT must exceed the single-photon coherence time (σ_{coh}) and the timing jitter (δT) of the detectors. It incorporates a time delay and coincidence measurements to reveal the JSI of entangled photons.[127] Since Franson measurements are temporal, their visibility is sensitive to the temporal phase of biphotons.[80,82,100] Conjugate Franson interferometry uses two MZIs with equal path differences and a frequency shift ($\Delta\Omega$) to eliminate local interference, applying a frequency shift of $\pm\Delta\Omega$ and non-local dispersion cancellation $\pm\beta_2$ ($\beta_2\Delta\Omega > \delta T$) to measure frequency domain coincidences, revealing the JTI of biphotons.[127,128] Combining both interferometries fully certifies energy-time entanglement by characterizing the biphoton wavefunction. While Franson interferometry measures JSI and temporal phase, conjugate Franson interferometry captures the spectral phase, providing a complete characterization of the quantum state. Dual-basis Franson interferometry can also be used for secure high-dimensional quantum key distribution (QKD).[127] These techniques are further discussed in a later section.

HIGH-DIMENSIONAL TIME-BIN ENTANGLEMENT IN QFCs

We now explore high-dimensional entanglement in QFCs, focusing on the time and frequency domains. Besides HOM revival interference measurements, Franson interferometry has also shown the revival of quantum interference, with the fringe reappearance period corresponding to multiples of the QFC's inverse frequency spacing[80,100,153] (Figure 4A). These discrete temporal revivals, due to mode locking, reveal high-dimensional energy-time entanglement. Franson interference directly measures the global coherence and energy-time correlations across different temporal modes in the QFC, provided that the QFCs are high-dimensional energy-time entangled in a non-local fashion. The high interference visibility (typically over 71%, for Bell inequality violation) in Franson interference patterns supports the high-dimensional energy-time entanglement in correlated frequency modes of QFC.

The temporal wavefunction of a QFC state has been described earlier in Equation 1. Consequently, QFC scaling to d dimensions can be achieved by increasing the FSR-to-bandwidth ratio of the cavity, allowing more time-bins with the same SPDC bandwidth. However, this leads to diminished Franson revival interference visibility due to the cavity's small finesse (Figure 4A). Figure 4B is the Schmidt mode eigenvalues that are calculated from the visibilities of HOM revival interferences, and the resulting Schmidt mode eigenvalues are smaller for lower interference visibilities. Hence, reduction of the HOM and Franson recurrence visibility will result in a lower dimensionality. This limits the scaling of entanglement of formation (E_{of}) and certifiable dimensionality in QFCs (Figure 4C). The entanglement of formation, E_{of}, quantifies entanglement and represents the minimum number of maximally entangled two-qubit states needed to create a density matrix, ρ. A certification of the dimensionality of the QFCs, it is described by:

$$E_{of} \geq -\log_2\left(1-\frac{B^2}{2}\right), \qquad \text{(Equation 2)}$$

where

$$B = \frac{2}{\sqrt{|C|}}\left(\sum_{\substack{(j,k)\in C \\ j<k}} |\langle j,j|\rho|k,k\rangle| - \sqrt{\langle j,k|\rho|j,k\rangle\langle k,j|\rho|k,j\rangle}\right), \qquad \text{(Equation 3)}$$

with ρ being the time-binned state's density matrix, and $|j,k\rangle$ being the biphoton key for the j^{th} signal time-bin and the k^{th} idler time-bin. In addition, C is the set of time-bin indices used in the sum, with $|C|$ being that set's cardinality.

This lower bound remains useful even with access to only a submatrix of the density matrix. For a $d\times d$ submatrix, a maximally entangled state has $B = \sqrt{2(d-1)/d}$, leading to $E_{of} = \log_2(d)$ ebits. In high-dimensional entanglement, this provides a quantitative lower bound, offering insights into the system's entanglement.[155] For qudit systems, E_{of} must exceed 1 ebit to surpass the two-dimensional qubit limit. For measurements in Figure 4A, E_{of} of 1.89 ± 0.03 ebits is certified for a local dimension of 16 in a 45 GHz FSR QFC, and an E_{of} of 1.40 ± 0.05 ebits is certified for the same local dimension in a 15 GHz FSR QFC.[100] Although ebits decline due to decreased Franson revival

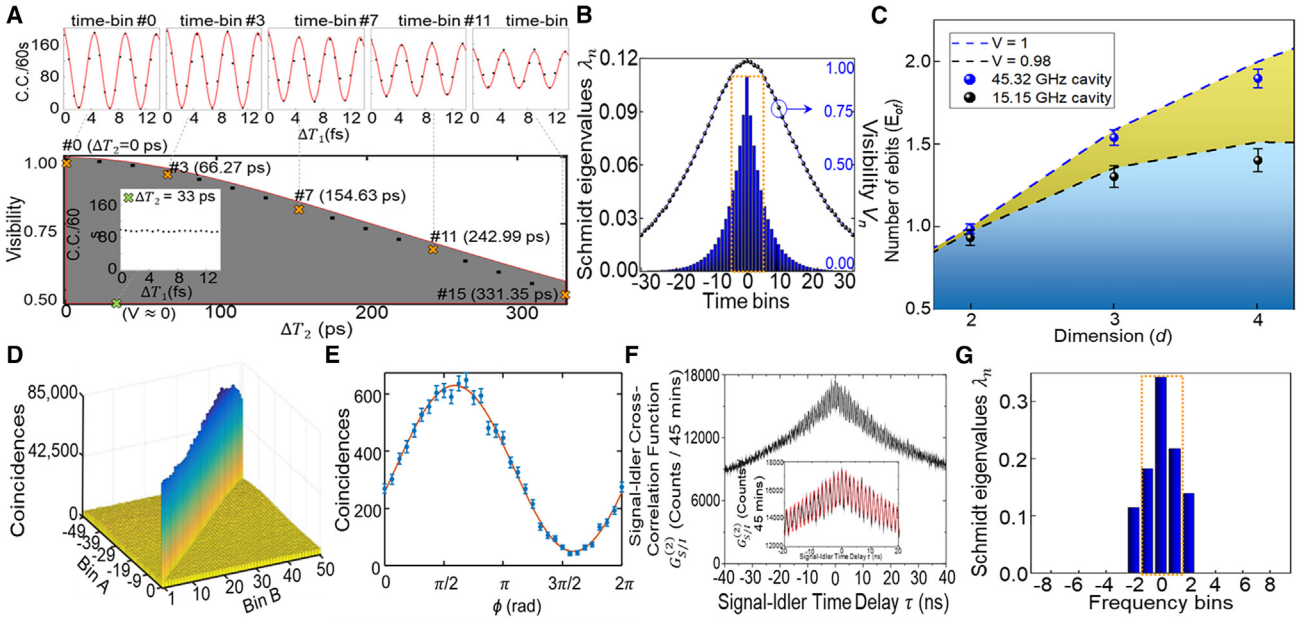

Figure 4. High-dimensional time-frequency entanglement in mode-locked QFCs

(A) Franson revival interferences using a mode-locked doubly-filtered QFC, demonstrating high-dimensional energy-time entanglement covering 16 time bins. C.C, coincidence counts. ΔT_1 is the fine time delay in one arm of the Franson interferometer. The inset is the comparison when the time delay is detuned from the cavity FSR, where there is no observable Franson fringes.

(B) The Schmidt mode eigenvalues (dark blue line) versus different time bins (histogram) from HOM interferometry and the corresponding visibilities of the HOM interference recurrences. Here, the Schmidt mode eigenvalues are calculated from the visibilities of HOM revival interferences.

(C) Lower bounds for the entanglement of formation (ebits) versus dimension d, in reconstructing the density matrix from Franson recurrence interference measurements.

(D) Measured frequency-correlated JSI of a mode-locked doubly-filtered QFC, with the measured Schmidt number K about 50.

(E) Frequency domain high-visibility interference as a function of spectral phase in a mode-locked QFC. Error bars denote the standard deviation predicted by Poissonian statistics.

(F) Time domain second-order cross-correlation measurements using a cavity-enhanced SPDC source. Inset is the zoom-in of the time domain second-order cross-correlation measurements.

(G) The Schmidt mode eigenvalues for measured QFC states from a 45 GHz FSR cavity. In (B) and (G), the dominant Schmidt mode eigenvalues for each high-dimensional BFC have been highlighted within the orange-dashed boxes and detailed in the supplemental information of Chang et al.[100] The measurements alone in (D) do not verify high-dimensional frequency-bin entanglement in QFCs; however, by incorporating measurements of frequency-bin mixing and temporal mode-locked oscillations in (E) and (F), they together certify the high-dimensional frequency-bin entanglement in QFC. The graphs in (A–C) and (G) are reprinted with permission from Chang et al.,[100] Springer Nature Limited. (D) Reprinted from Lu et al.,[86] OSA. (E) Reprinted from Lu et al.,[93] Springer Nature Limited. (F) Reprinted from Scholz et al.,[154] APS.

interference visibility, this can be improved with a cavity of higher finesse and reasonable Q-factor (typically 10^5 to 10^7 in telecom wavelengths) under the same FSR.[91,101,156–158] However, increasing cavity finesse improves Franson recurrence visibility but requires longer temporal delays for probing more time-bins. For even larger delays, the size of the fiber interferometer and its temperature stability become issues; a free-space bulky Franson interferometer[155,159–161] could be used but needs active stabilization feedback for phase-sensitive non-local quantum interferences.

The scalability of high-dimensional time-bin entanglement is limited by detection capabilities, the number of interferometers, imbalances within interferometers, and the timing jitter of single-photon detectors. For instance, although the quantum state tomography can provide complete characterization of a four-dimensional time-bin qudits state[162]; however, the number of required interferometers scales linearly with the number of time-bins or dimensionality d.[163] Certifying high-dimensional or multipartite entanglement with a limited number of measurements is challenging, as quantum-state tomography becomes extremely time-consuming or unavailable for complex states.[164] Alternatively, high-dimensional time-bin entanglement in QFCs can be certified by using a reasonable number of measurements on the Franson interference fringes, and the theoretical assumptions on the quantum states, to derive the lower bound estimation of E_{of}.[100,155,158] Similarly, multiple Franson interference fringes from QFCs can be used to provide the witness of qudit time-bin entanglement by violating the Bell inequality[80–84,100]; however, this method is limited to verifying entanglement, but not full characterization of the quantum state. Another recent method is to find and measure mutually unbiased basis (MUBs) for certain dimensionality d, which requires no full quantum state tomography for high-dimensional time-bin entanglement certification.[163,165–173] In a Hilbert space of dimensionality

d, MUBs consist of orthonormal bases where the inner product between states from different bases equals $1/d$. Measurements in one MUB provide no information about a state prepared in another, due to quantum uncertainty.[168,169] For a d-dimensional subspace, there are d+1 sets of MUBs.[165] The limitation of this method is that it typically requires high-precision spectral or temporal measurements to estimate MUBs.

On the application side, finding the correct MUBs is crucial for prepare-and-measure QKD schemes such as BB84.[167] There are three main approaches for finding MUBs in energy-time DoF: inserting equal amplitude but opposite sign group velocity dispersions on biphotons,[170,171] using multiple Franson interferometers,[163,172] or employing a cascade of electro-optic phase modulators.[173] Each method has its strengths and challenges, such as insertion loss, alignment, and scaling.[166] Entanglement-based QKD protocols, however, do not require MUB measurements and use quantum non-local interferometry for entanglement characterization.[6,127,174] Franson-type interferometry can test Bell's inequality and set upper limits on Eve's Holevo information leakage.[5,175,176] While past work used single-photon detectors with timing jitter in the range of tens to hundreds of ps, recent advances with SNSPDs achieving sub-3 ps resolution[56] are expected to enhance the exploration and scaling of high-dimensional time-bin entanglement for applications such as quantum communication and computing.

HIGH-DIMENSIONAL FREQUENCY-BIN ENTANGLEMENT IN QFCs

In QFCs, mode locking occurs simultaneously in both the time and frequency domains. Notably, the resulting spectral correlation from these quantum combs is discrete rather than continuous (Figure 4D). Complementary to Equation 1, the spectral wavefunction of the QFC is written as:

$$|\psi\rangle = \sum_{m=-N_0}^{N_0} \int d\Omega\, f'(\Omega) f(\Omega - m\Delta\Omega) \hat{a}_H^\dagger\left(\frac{\omega_p}{2} + \Omega\right) \times \hat{a}_V^\dagger\left(\frac{\omega_p}{2} - \Omega\right)|0\rangle, \quad \text{(Equation 4)}$$

where ω_p is the frequency of pump photon, $f'(\Omega)$ is the $\mathrm{sinc}(Am\Delta\Omega)$ in Equation 1, $f(\Omega - m\Delta\Omega)$ is the single frequency-bin profile defined by the cavity's Lorentzian transmission lineshape with FWHM linewidth $2\Delta\omega$, as $f(\Omega) = 1/[(\Delta\omega)^2 + \Omega^2]$. Since 2014, high-dimensional frequency-bin entanglement in QFCs has gained significant attention as previous limitations in mixing and manipulating multiple frequency-bins have been lifted. With the introduction of frequency-bin control,[177] Fourier transform pulse shapers and electro-optic phase modulators have become key tools for complex quantum information processing and quantum computing in QFCs.[83,86–89,95] Pioneered by Weiner,[109,178] pulse shapers act as user-programmable filters for spectral amplitude and phase, while phase modulators facilitate frequency-bin superposition measurements. Cascading these tools allows for unitary and universal gate operations on multiple frequency-bins.[86,88,89]

Besides generation and control, certifying high-dimensional frequency-bin entanglement is crucial. Solely measuring JSI for frequency-correlation (Figure 4D) is inadequate due to unknown spectral phase coherence. Certification can be achieved by measuring spectral phase coherence via quantum interference after mixing frequency-bins[93] (Figure 4E), or using JSI with complementary JTI measurements[154] (Figure 4F). In addition, HOM and Franson revival interference measurements, combined with JTI measurements, can further confirm high-dimensional entanglement.[153] Schmidt mode decompositions are also used to quantify dimensionality by extracting the Schmidt number K from the JSA or JTA. The Schmidt number K is defined as:

$$K = \left(\sum \lambda_n^2\right)^{-1}, \text{where} \sum \lambda_n = 1, \quad \text{(Equation 5)}$$

with $\{\lambda_n\}$ being the Schmidt mode eigenvalues. For frequency- or time-bins, Schmidt eigenvalues come from the frequency-binned JSA or time-binned JTA. Directly measuring JSA and JTA is challenging due to the need to reconstruct complete phase information. Instead, JSI and JTI measurements are used to estimate the Schmidt number, assuming a pure quantum state.[82,83,100] The Schmidt number K measures the number of correlated modes in a quantum state[179,180] (Figure 4G). The discrete multi-mode nature of mode-locked QFCs allows quantification of their Hilbert space dimensionality through Schmidt mode decompositions in frequency and time domains.[82,83,100] Although the Schmidt number K reflects frequency-correlation and correlated modes, it requires knowledge of the spectral phase from JSA. The frequency domain Schmidt number K can represent quantum dimensionality in QFCs with direct JTI measurements or frequency-bin mixing. High-dimensional correlated frequency-bins has been demonstrated in QFCs,[85,86,93] with a measured Schmidt number K of approximately 20 in a 50 GHz FSR QFC and about 50 in a 25 GHz FSR QFC.[85,86] Recently, an E_{of} of 2.198 ± 0.007 ebits is certified in a 40 GHz FSR QFC, and an E_{of} of 2.50 ± 0.08 ebits is certified in a 40.5 GHz FSR integrated QFC using high-dimensional frequency-bin encoding and Bayesian tomography.[93]

Besides the QFCs based on two photons, the generation of a multi-photon energy-time entangled state using integrated QFCs has been demonstrated.[81,83] First, in Figure 5A, the single-photon frequency spectrum of an integrated QFC is measured from telecom S to L band. Six frequency-bin pairs have been measured with raw entanglement visibility over 80%. Each photon of the spectrally filtered frequency-bin pair from an on-chip QFC is individually passed through an unbalanced fiber interferometer with the temporal imbalance equal to the time-bin separation of the two pulses for quantum-state tomography measurements. The measured quantum interference and density matrix of the four-photon entangled qudit state are 89% and 64% (Figure 5B), respectively. Later, the same group demonstrated the generation and coherent control of an integrated 10-dimensional QFC using pulse shapers and electro-optic phase modulators (Figure 5C). Then, they performed quantum-state tomography of high-dimensional frequency-bin qudit states (d = 3 and 4), with quantum inference visibility of 86.6% and 86.4%, and with quantum state fidelity of 80.9% and 76.6% (Figure 5D), respectively. These works highlight the scalability of multi-photon QFC state, as it can be

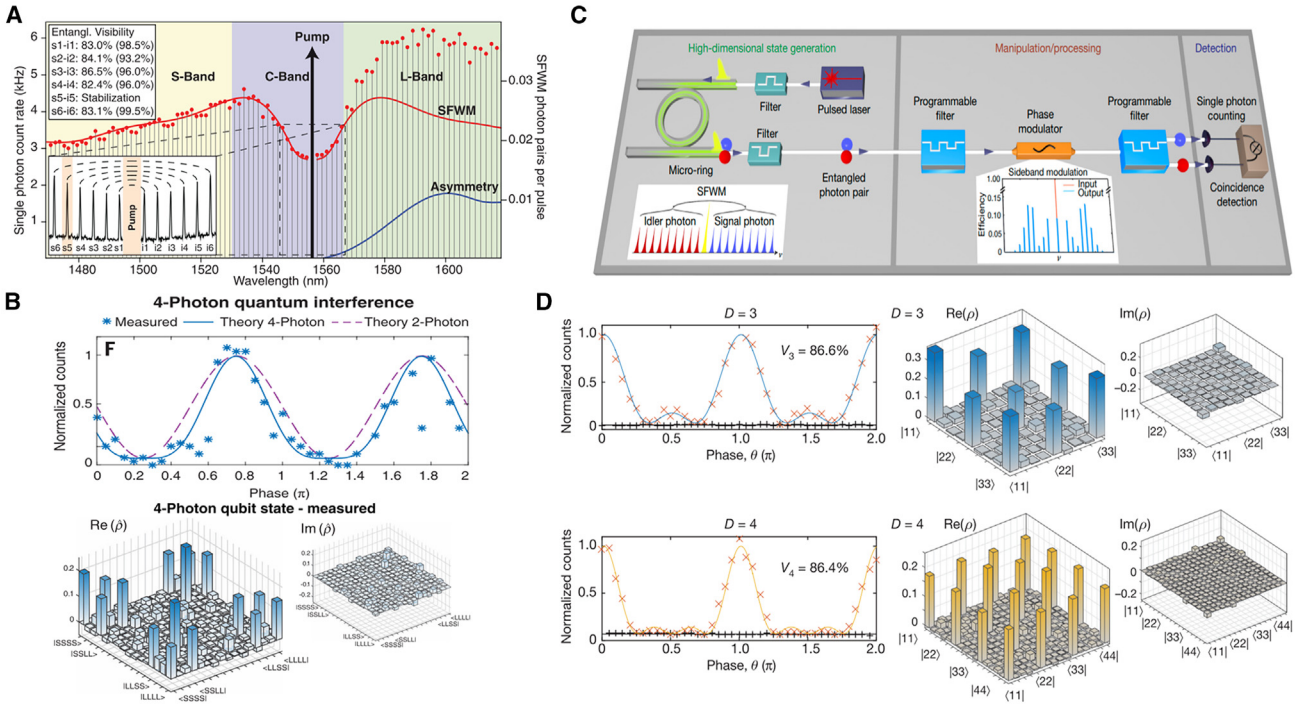

Figure 5. High-dimensional time-frequency entanglement in integrated QFCs

(A) The measured frequency spectrum of integrated QFC in a Hydex four-port microring resonator.

(B) Full quantum-state tomography measurements of a four-photon time-frequency entangled states. The measured quantum interference and density matrix of the four-photon entangled qudit state are 89% and 64%, respectively.

(C) The experimental setup for coherence control of on-chip QFC.

(D) Quantum-state tomography of high-dimensional frequency-bin qudit states (d = 3 and 4), with quantum inference visibility of 86.6% and 86.4%, and with quantum state fidelity of 80.9% and 76.6%, respectively. The graphs in (A) and (B) reprinted with permission from Reimer et al.,[81] AAAS. (C and D) Reprinted from Kues et al.,[83] Springer Nature Limited.

generated and controlled using commercial telecom components and integrated on-chip devices.[81,83]

Here, we briefly summarize different methods for high-dimensional frequency-bin entanglement certification using QFCs. Quantum-state tomography provides full characterization of the qudit state, but it comes with the cost of exponentially increasing the number of measurements as dimensionality d increases. The other method is to use quantum interference fringes for frequency qudit state of QFCs to violate the Bell inequality; however, this method is limited to verifying entanglement instead of full characterization of the quantum state. Another method to certify high-dimensional frequency-bin entanglement in QFCs is to use random phases from pulse shaper, prior knowledge of the quantum state, and Bayesian tomography to derive the lower-bound estimation of E_{of}.[93] The high-dimensional frequency-bin certification for QFC state can be achieved by measuring spectral phase coherence via quantum interference after mixing frequency-bins,[83,85,86,93] with the limitation on the optical loss in the process of frequency-bin superposition. The other recent method for witnessing qudit frequency-bin state of QFCs is via using JSI and complementary JTI measurements, where the spectral phase information is provided in the JTI measurements.[153,158] This method has limitation on the JTI measurements, which is due to the timing resolution of single-photon detectors.

The scalability of high-dimensional frequency-bin entanglement is influenced by several factors, including the number of elements, bandwidth for electro-optic phase modulators, cavity FSR, and insertion loss per element (typically a few dB in telecom wavelengths). As with high-dimensional energy-time and time-bin entanglement, the number of elements increases linearly with the number of frequency-bins or dimensionality (d) of the entangled system. Modulation efficiency tends to decrease as dimensionality increases.[181] While commercially available devices typically have a bandwidth limit of 50 GHz, cutting-edge electro-optic phase modulators now reach 100 GHz,[182,183] with further improvements expected. Alternatively, using smaller FSR QFCs also scales the dimensionality d of high-dimensional frequency-bin entanglement. For instance, several studies have demonstrated high-dimensional frequency-bin entanglement with cavities having FSRs smaller than 50 GHz.[86,93,100] On-chip integration techniques can help mitigate coupling loss in electro-optic phase modulators, pulse shapers, and frequency shifters.[182,184,185]

FRANSON AND CONJUGATE FRANSON INTERFEROMETRY

Franson and conjugate Franson interferometry are key methods in quantum information science for characterizing and verifying

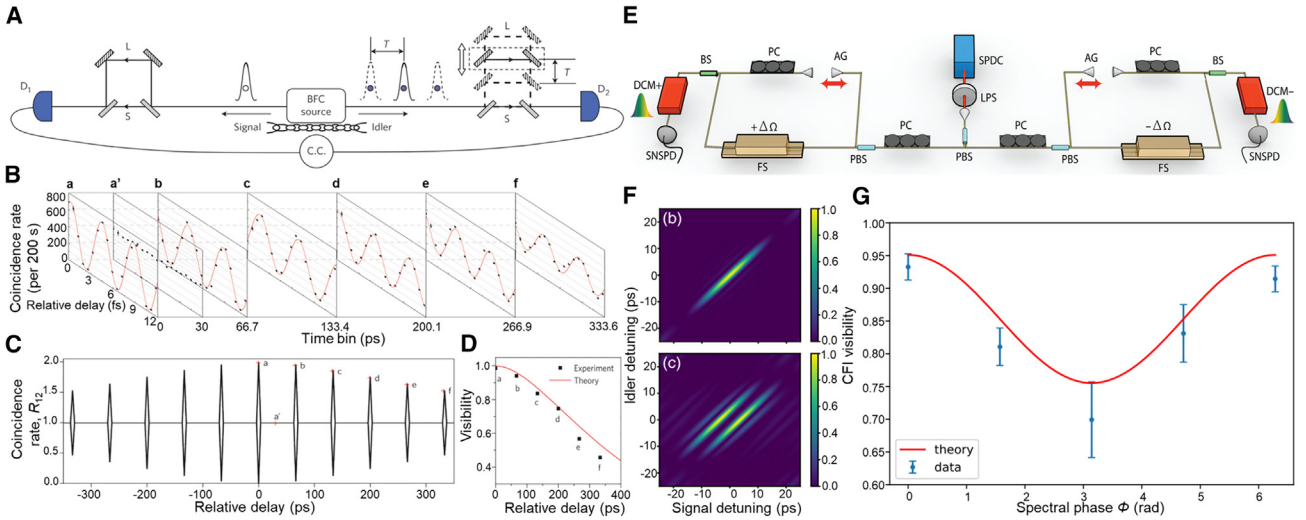

Figure 6. Franson and conjugate Franson interferometry for high-dimensional time-frequency entanglement verification

(A) Experimental scheme of Franson interferometer to verify high-dimensional energy-time entanglement in a QFC state.

(B) The first Franson revival interferences measured in a mode-locked QFC, demonstrating high-dimensional energy-time entanglement covering six resonances where a–f indicate discrete time-bin positions.

(C) Theoretical fringe envelope of Franson interference revivals for a QFC, with superimposed experimental data.

(D) Comparison of experimental and theoretical visibility of high-dimensional Franson interference fringes as a function of time delay, with central Franson visibility of 97.8% after accidental subtractions.

(E) Experimental setup of the conjugate Franson interferometer, comprising two MZIs with equal length arms and an optical frequency shifter placed in one arm of each MZI.

(F) JTI of a biphoton state with different spectral phases 0/2 π (upper) and π (lower).

(G) Conjugate Franson fringe visibility as a function of spectral phase. The current experimental conjugate Franson interference (CFI) visibility is 96% ± 1% without background subtraction. The conjugate Franson interference visibility degrades when spectral phase variation is introduced. Error bars represent one standard deviation of three measurements. The graphs in (A)–(D) are reprinted with permission from Xie et al.,[80] Springer Nature Limited. (E–G) Adapted with permission from Chen et al.,[128] APS.

the joint high-dimensional time-frequency entanglement, essential for advanced quantum communication and computing. These techniques use quantum superposition and interference principles to explore entanglement across multiple time- and frequency-bins, deepening our understanding of these quantum systems.[100,153,155,156]

Franson interferometry,[152] introduced by James Franson in 1989, involves a two-path interferometer where a photon pair, generated via SPDC, is split and sent through two unbalanced MZIs (Figure 6A). The pathlength difference introduces a relative time delay, enabling the measurement of two-photon interference patterns from indistinguishable temporal paths. This setup measures energy-time entanglement and coherence between photons. Recent demonstrations of Franson revival interferences[80] utilize tunable delays across multiple time-bins at the integer of the cavity, with central Franson visibility of 97.8% after accidental subtractions. This experiment provides the high-dimensional energy-time entanglement with interference recurrence visibilities in a QFC (Figures 6B–6D). Conjugate Franson interferometry extends this approach by incorporating dispersive elements that introduce frequency-dependent delays[127,128] (Figure 6E). This allows control of interference patterns in the time domain and examination of entanglement in conjugate time-frequency variables, verifying spectral phase coherence with the same JSI but different JTI (Figures 6F and 6G). Currently, the highest experimental conjugate Franson interference visibility achieved is 96% ± 1% without background subtraction.[128] Moreover, the theoretical conjugate Franson recurrence interference visibilities for the entangled QFC state is given in Chang et al.,[100] providing another method for certification of high-dimensional frequency-bin entanglement in QFCs. These methods are crucial for probing quantum mechanics and have practical implications for quantum technologies. They enhance the performance and security of quantum communication, allowing greater information transmission per photon and resilience against eavesdropping.[127] In addition, they are vital for developing quantum computing architectures using time-frequency modes as qudits, advancing large-scale quantum information processing.

HIGH-DIMENSIONAL TIME-FREQUENCY ENTANGLEMENT IN QFCs

Hyperentanglement involves correlation of all accessible DoFs between two or more particles, including time, frequency, spin angular momentum (polarization), and orbital angular momentum.[186] For example, the *d*-level quantum states involving multiple particles are often created using Greenberger-Horne-Zeilinger (GHZ) states with orbital angular momentum. These are typically generated in bulk free-space setups,[67,187] but suffer from reduced coherence time and detection rates, bounding the realization to 27-dimensional spaces.[187] In contrast, multimode

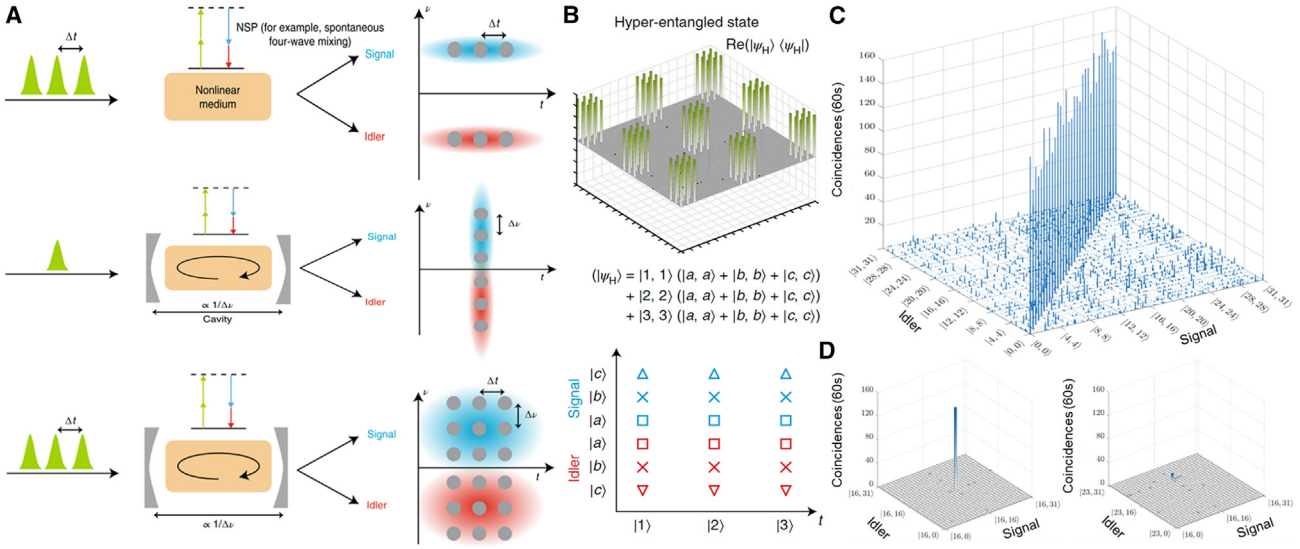

Figure 7. Hyperentanglement in mode-locked QFCs

(A) Time-frequency hyperentanglement generation scheme. An optical pulse train excites a nonlinear medium to generate a time-bin entangled two-photon state. A single pulse excites a nonlinear medium in a cavity to generate photon pair over a broad bandwidth, i.e., a frequency-bin entangled state. An optical pulse train excites a nonlinear medium in a cavity to generate a simultaneously time- and frequency-bin entangled state, i.e., a time-frequency hyperentangled state.
(B) An example two-photon time-frequency hyperentangled state comprising three temporal modes and three frequency modes per signal and idler photon.
(C) The demonstration of a four-party 32-dimensional GHZ state using a high-dimensional gate operation for hyperentangled QFC, encoding up to 20 qubits.
(D) Zoomed-in submatrices of matched and unmatched signal and idler frequency-bins in (C). The graphs in (A) and (B) were adapted with permission from Reimer et al.,[87] Springer Nature Limited. (C and D) Adapted with permission from Imany et al.,[89] Springer Nature Limited.

time- and frequency-bin entanglement allows the creation of hyperentangled states, such as a four-party high-dimensional GHZ state[89] or a three-level four-partite cluster state,[87] using only QFCs without extra particles. High-dimensional entanglement in QFCs involves connecting time-bin and frequency-bin observables, two discrete forms of energy-time entanglement. High-dimensional time-frequency entanglement can serve as the foundation for time-frequency hyperentanglement. For example, these states can be created by exciting SPDC or spontaneous four-wave mixing mediums with multiple temporal pulses (Figure 7A). The key requirement is that pulse separation must exceed the cavity photon lifetime to achieve a time-frequency product greater than the EPR limit ($\Delta\nu\Delta t \gg 1$, where $\Delta\nu$, Δt represent the frequency and time spacing between different modes), allowing independent control of time- and frequency-bins (Figure 7B).[152,188] Time-frequency entanglement requires a pulsed pumping scheme, as continuous-wave pumping aligns cavity round-trip time with frequency spacing, yielding $\Delta\nu\Delta t = 1$. Figure 7B is an experimental example of a two-photon time-frequency hyperentangled state, consisting of three temporal modes and three frequency modes per signal and idler photon.[87] Recent experimental demonstrations using a controlled-NOT gate and entangled states show a four-party GHZ state with 32 dimensions per DoF[89] (Figures 7C and 7D), corresponding to a Hilbert dimensionality of 32^4, equivalent to 20 qubits. However, this GHZ state, while realized using QFCs, is not directly applicable for genuine multi-party GHZ applications, such as Mermin inequality violations.[187,189]

Hyperentanglement by combining temporal or spectral modes with other DoFs is helpful for implementing deterministic controlled-NOT gates,[190–195] foundational for applications such as dense quantum coding,[80,100,196] high-dimensional quantum networks,[197,198] efficient quantum memory storage,[199] and superdense quantum teleportation.[200] Specifically, entanglement in QFCs has been demonstrated for time-frequency,[87] energy-time polarization,[80] and frequency polarization DoFs.[101,102] An on-chip QFC has also been integrated into a Sagnac interferometer to generate hyperentanglement with frequency polarization DoFs.[102] High-dimensional time-frequency entanglement in QFCs leverages its multiple temporal and spectral mode structure, compatible with fiber optical technology. This approach enhances noise tolerance and increases the effective quantum resource rate, enabling advanced and robust quantum computations.

DOUBLY AND SINGLY-RESONANT CAVITY-ENHANCED QFCs

The mode-locked QFCs discussed above operate in a doubly-resonant (DR) configuration, where the signal and idler photon spectra are confined within the cavity modes simultaneously (Figure 2A). Since the first cavity-enhanced SPDC source was demonstrated,[76] many studies have focused on DR-OPO schemes operated far below threshold.[201–210] This approach enhances the biphoton flux by a factor of cavity finesse and the brightness by the square of the finesse.[211] The bandwidth of these sources typically ranges from a few MHz to 100 MHz,[212] useful for integrating quantum memory with atomic ensembles whose bandwidth is 10–100 MHz.[213] However, this scheme faces stability issues due to maintaining resonance conditions

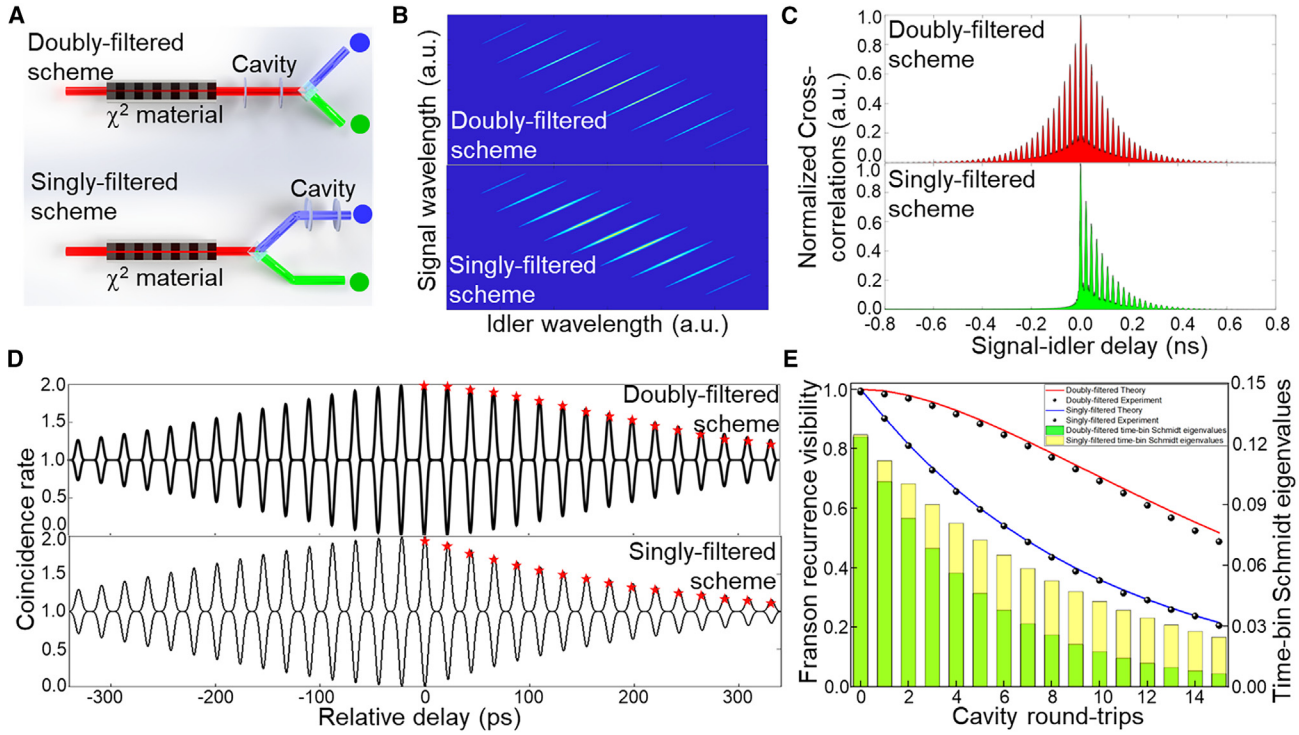

Figure 8. Mode-locked doubly- and singly-filtered QFCs

(A) Schemes for mode-locked doubly- and singly-filtered QFCs.

(B) Example JSI of doubly- and singly-filtered QFCs. While the FSR of comb structures remains consistent across doubly- and singly-filtered schemes in the frequency domain, their JSI exhibits two notable distinctions. First, in doubly-filtered QFC, the JSI has a more rapid decay as the frequency offset from the comb center increases, contrasting with the singly-filtered scheme. Second, the singly-filtered QFC displays a higher unnormalized power spectral intensity compared with the doubly-filtered configuration.

(C) Modeled signal-idler cross-correlation $g^{(2)}$ function (cross-section of JTI) of doubly- and singly-filtered QFC. Here, the signal-idler cross-correlation $g^{(2)}$ functions exhibit double- and single-sided temporal oscillating structures with a detection timing jitter δT of 5 ps.

(D) The experimental and theoretical visibilities of the Franson revival interference fringes in mode-locked doubly- and singly-filtered QFC. The coincidence counts in Franson interference experiments are superimposed for 16 positive time bins. (E) The Franson recurrence visibility and corresponding time-bin Schmidt eigenvalues for mode-locked doubly- (red line and yellow bar) and singly-filtered (blue line and green bar) QFCs. The graphs and data in (D) and (E) are reprinted with permission from Chang et al.[100] and Cheng et al.,[153] Springer Nature Limited.

for both signal and idler beams under varying parameters. An improved method is using a triply resonant SPDC source, which reduces the FSR and bandwidth, simplifying cavity locking and enhancing stability.[111,154,214,215]

On the other hand, singly-resonant (SR) QFCs have been proposed[211] and demonstrated in cavity-enhanced SPDC sources.[91,100,216,217] Due to the entanglement between the signal and idler photons, both will display comb-like spectra,[91,100,216] even if only one photon is resonant with the cavity mode. SR cavity-enhanced SPDC is more stable and tunable since only one photon interacts with the cavity. However, the brightness of an SR-OPO is typically lower than a DR-OPO, as the cavity only enhances one type of photon and does not amplify the total photon flux due to losses within the cavity. SR schemes also avoid the cluster effect common in DR-OPO configurations,[91,101] which suppresses photon pair generation due to the frequency dependency of FSR.[218,219] A recent review provides mathematical formulas and detailed implementations of cavity-enhanced SPDC sources.[212] Although the bandwidth of DR and SR cavity-enhanced QFCs in SPDC sources is suitable for atomic quantum memories,[220–223] the typical FSR is not compatible with commercial optical filters and modulators, limiting single-mode control and applications in quantum communications and computings.

DOUBLY AND SINGLY-FILTERED QFC

Since 2015, versatile QFCs that can be configured in both doubly- and singly-filtered approaches have been investigated.[80,100,153] In this setup, switching between these configurations can be done within a single experiment, avoiding the need to rebuild and stabilize the system (Figure 8A). This is feasible for QFCs based on post-filtering, as the cavity mode structure can be applied to both biphotons simultaneously or to only signal or idler photons. The JSI shaping of type II SPDC photons can be achieved by inserting a cavity before splitting the photons, which is the doubly-filtered configuration[80,100] (Figure 2C). Conversely, changing the location of the splitting component enables singly-filtered operation by affecting only the spectrum of signal or idler photons, preserving the mode-locked QFC

signature due to intrinsic photon pair entanglement.[153,156] The JSI for both configurations is then compared (Figure 8B). For doubly-filtered QFCs, its unnormalized frequency domain wavefunction is:

$$\psi_{\text{Doubly}-\text{filtered}}(\Omega) = \sum_{m=-N}^{N} \frac{\text{sinc}(A\Omega)}{|\Delta\omega + i(\Omega - m\Delta\Omega)|^2} \quad \text{(Equation 6)}$$

For the singly-filtered configuration, its unnormalized frequency domain wavefunction is:

$$\psi_{\text{Singly}-\text{filtered}}(\Omega) = \sum_{m=-N}^{N} \frac{\text{sinc}(A\Omega)}{\Delta\omega + i(\Omega - m\Delta\Omega)} \quad \text{(Equation 7)}$$

Although the FSR of the comb structure is the same for both doubly- and singly-filtered schemes, their JSI differs in two ways. First, in the doubly-filtered case, where both the signal and idler photons are filtered, the frequency domain biphoton wavefunction decays faster with increasing frequency offset compared with the singly-filtered configuration. Second, the power spectrum differs: the singly-filtered QFC has a higher unnormalized power spectral intensity than the doubly-filtered QFC (Figure 8B). The JSI fall-off can be improved by using SPDC with a larger phase-matching bandwidth or a cavity with a smaller FSR. Singly-filtered QFCs also have higher photon flux than doubly-filtered ones, with no cavity enhancement for either scheme. This difference in JSI results in different JTI for the two post-filtering schemes. For the doubly-filtered scheme, the unnormalized temporal domain wavefunction is:

$$\Psi_{\text{Doubly}-\text{filtered}}(|n|\Delta T) = \exp(-|n|\Delta\omega\Delta T) \sum_{m=-N}^{N} \text{sinc}(Am\Delta\Omega) \quad \text{(Equation 8)}$$

whereas for the singly-filtered configuration, its unnormalized temporal domain wavefunction is:

$$\Psi_{\text{Singly}-\text{filtered}}(n\Delta T) = \exp(-n\Delta\omega\Delta T) \sum_{m=-N}^{N} \text{sinc}(Am\Delta\Omega) \quad \text{(Equation 9)}$$

The QFC state's temporal behavior exhibits recurrences with a period inverse to the comb spacing. Doubly-filtered QFCs show double-sided signal-idler cross-correlation $g^{(2)}$ functions,[100] while singly-filtered QFCs show single-sided $g^{(2)}$ functions.[153,156,211] For a 45 GHz FSR fiber cavity, efficient generation of both doubly- and singly-filtered QFCs can be achieved. These exhibit double- and single-sided temporal oscillations (Figure 8C) with a detection timing jitter δT of 5 ps, achievable with state-of-the-art SNSPDs.[56] Recent observations using Franson interferometry have revealed high-dimensional energy-time entanglement in both QFC types[100,153,156] (Figure 8D). In singly-filtered QFCs, where only the signal photons pass through the cavity, Franson recurrences show faster fall-off for positive temporal delays compared with doubly-filtered QFCs. Despite the single-sided $g^{(2)}$ function, the Franson revival interferences cover both positive and negative delays due to the overlap integral with the delay-shifted counterpart.[153] The visibility of Franson recurrences at positive time-bins decreases faster than at negative time-bins, due to the asymmetric temporal profile of the cross-correlation function.[153,156] The relationship between Franson revival visibility and time-bin Schmidt number K_T is not fully understood, although recent investigations suggest a link with the two-photon JSI and corresponding Schmidt number.[224,225] Understanding this connection involves analyzing the visibility of the n^{th} Franson interference recurrence. The visibility of the n^{th} Franson interference recurrence in the doubly-filtered scheme is:

$$V_{n\ (\text{Doubly}-\text{filtered})} = \exp(-|n|\Delta\omega\Delta T)(1 + |n|\Delta\omega\Delta T) \quad \text{(Equation 10)}$$

Subsequently, the visibility of the positive n^{th} Franson interference recurrence for singly-filtered configuration can be described as:

$$V_{n\ (\text{Singly}-\text{filtered})} = \exp(-n\Delta\omega\Delta T) \quad \text{(Equation 11)}$$

where $\Delta T = 2\pi/\Delta\Omega$ is the repetition rate of QFCs. Then, the time-bin Schmidt eigenvalues λ_n can be extracted via the following expression for doubly-filtered QFCs:

$$\lambda_{n\ (\text{Doubly}-\text{filtered})} = \frac{e^{-\pi|n|/F}}{\sum_{n=-M}^{M} e^{-\pi|n|/F}}, 0 \le |n| \le M \quad \text{(Equation 12)}$$

In singly-filtered QFC, the time-bin Schmidt eigenvalues λ_n is:

$$\lambda_{n\ (\text{Singly}-\text{filtered})} = \frac{e^{-\pi n/F}}{\sum_{n=0}^{M} e^{-\pi n/F}}, \text{for } 0 \le n \le M \quad \text{(Equation 13)}$$

where $M + 1$ is the number of time-bins from Franson revival interferences, and F is the cavity finesse. In both schemes, the time-bin Schmidt number K_T can be extracted using Equation 3. The symmetric and asymmetric Franson recurrence interferences in doubly- and singly-filtered schemes arise from their unnormalized temporal wavefunctions. The experimental Franson revival interference visibilities and time-bin Schmidt eigenvalue λ_n in both configurations, with measured K_T values of 13.11 (13.19 theoretical) and 20.72 (21.04), respectively (Figure 8E). The temporal wavefunctions of QFCs suggest that improving the Franson visibility decay and K_T could be achieved with a cavity of larger finesse F given a fixed FSR.[156]

In Table 1, we summarize recent key experimental QFC demonstrations from various configurations. Both the doubly- and singly-filtered configurations in QFCs offer their own set of advantages and disadvantages. For instance, the singly-filtered configuration exhibits a higher photon flux compared with the doubly-filtered configuration. As a result, it is more beneficial to employ the singly-filtered QFCs for quantum communication applications such as high-dimensional entanglement distribution and wavelength-multiplexed QKD.[153] Notably, singly-filtered QFC can also be utilized for applications such as multimode quantum memory storage.[209,226–228] The singly-filtered configuration provides increased stability and greater tunability, making

Table 1. Comparison of recent quantum frequency combs

Process	Platform	Configuration	λ (nm)	Encoding	Photons	Frequency modes	Temporal modes	Schmidt number	ebits	Focus	Reference
SPDC	PPKTP	doubly-filtered	1,316 + 1,316	energy-time polarization	2	10	19	/	/	high-dimensional hyperentanglement QFC	Xie et al.[80]
SPDC	PPKTP	DR	795 + 795	time-bin	2	~800	84	/	/	hectometer HOM revivals in a QFC	Rambach et al.[111]
SFWM	glass	DR	~1,550	time frequency	2–4	10	10	10.45 ± 0.53	/	on-chip generation and coherent control of high-dimensional QFC	Kues et al.[83]
SFWM	Si_3N_4	DR	~1,550	time frequency	2	40	/	20	/	50 GHz spacing on-chip QFC	Imany et al[85]
SPDC	PPLN	doubly-filtered	~1,550	time frequency	2	50	/	/	/	frequency-bin HOM interference in a QFC	Lu et al.[86]
SPDC	PPLN	doubly-filtered	~1,550	time frequency	2	50	/	/	/	frequency CNOT gate using a QFC	Lu et al.[88]
SPDC + SFWM	PPLN + Si_3N_4	doubly-filtered + DR	~1,550	time frequency	2	256	256	/	1.19 ± 0.12	bipartite GHZ state with a Hilbert space of 20 qubits in a QFC	Imany et al.[89]
SPDC	PPLN	SR	1,520–1,600	time frequency	2	1,000	~30	/	/	a broadband multimode QFC	Ikuta et al.[91]
SPDC	PPLN	doubly-filtered	~1,550	time frequency	2	50	/	/	/	high-dimensional quantum walk with a QFC	Imany et al.[95]
SPDC	AlGaAs	doubly-filtered	~1,530	time frequency	2	500	/	/	/	integrated semiconductor QFC source	Maltese et al.[98]
SPDC	PPKTP	doubly-filtered	1,316 + 1,316	time frequency polarization	2	19	61	18.30	1.89 ± 0.03	a 648 Hilbert space dimensional QFC	Chang et al.[100]
SPDC	PPLN	SR	1,520–1,600	time frequency	2	1,400	~30	10	/	massive mode polarization entangled QFC	Yamazaki et al.[101]
SPDC + SFWM	PPLN + Si_3N_4	doubly-filtered + DR	~1,550	time frequency	2	51	/	/	2.50 ± 0.08	frequency-bin quantum state tomography using QFCs	Lu et al.[93]
SPDC	PPKTP	singly-filtered	1,316 + 1,316	time frequency	2	5	16	13.11	/	high-dimensional entanglement distribution and QKD with singly-filtered QFC	Cheng et al.[153]

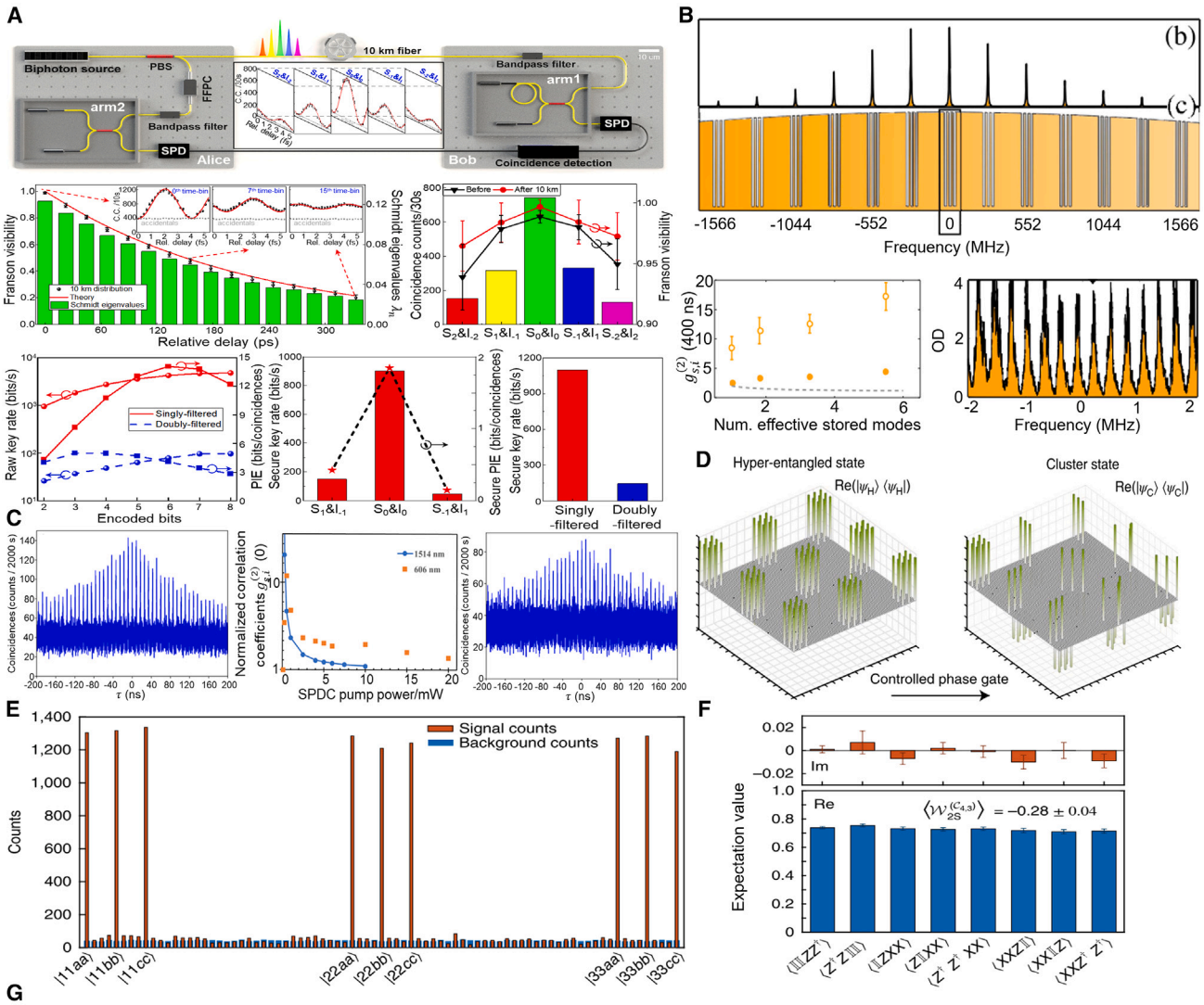

G

Pump source	Encoding	Entanglement distribution	Quantum key distribution	Quantum storage	Quantum computation	Notes	Reference
CW	Time-bin	Yes	Yes	No	No	First entanglement distribution and high-dimensional QKD using singly-filtered QFC	[155]
CW	Polarization	Yes	No	No	No	16 frequency-multiplexed channels using 25 GHz DWDM in a QFC	[248]
CW	Polarization	Yes	No	No	No	A wavelength-converted entanglement distribution using a QFC	[255]
CW	Time-frequency	No	No	Yes	No	First frequency-multiplexed quantum storage of a QFC	[210]
Pulsed	Time-frequency	No	No	No	Yes	First *d*-level cluster states using an on-chip QFC	[87]

Figure 9. Quantum communications and computation processing with mode-locked QFCs

(A) An efficient entanglement distribution using time- and frequency-bins of a mode-locked singly-filtered QFC after a 10-km fiber link. Proof-of-principle high-dimensional QKD using mode-locked singly- and doubly-filtered QFC has also been demonstrated. $S_0\&I_0$, $S_1\&I_{-1}$, and $S_1\&I_1$ are the selected frequency-bin pairs in a singly-filtered QFC. The error bars represent one standard deviation of the mean assuming Poissonian statistics.

(B) Matched atomic frequency comb and DR-OPO spectrums, and the measured second-order cross-correlation function [$g^{(2)}_{s,i}$ (400 ns)] for stored frequency-multiplexed BFC. OD is the optical depth. Error bars are from Poissonian statistics.

(C) The temporal multimode nature (from second-order cross-correlation function [$g^{(2)}_{s,i}$ (0)]) of a wavelength-converted DR-OPO with 10-km fiber. τ is the relative delay between signal and idler.

(D) Generation of *d*-level cluster states from time-frequency hyperentangled state with a controlled phase gate.

(E) Measured photon projections on the 81 diagonal elements of the cluster-state density matrix.

(legend continued on next page)

it suitable for a broader range of non-degenerate or degenerate heralding measurements. In contrast, doubly-filtered QFCs overall have better two-photon interference visibility and Hilbert space dimensionality, and are more suitable for time-frequency high-dimensional entanglement state generations toward cluster state quantum computations[86,89] and for Sagnac interferometry[229,230] with frequency polarization entanglement in higher-dimensional dense encoding.[80,100]

The doubly- and singly-filtered QFCs offer greater versatility compared with cavity-enhanced SPDC sources. These mode-locked QFCs, implemented with post-filtering cavities, utilize telecom fiber components and do not necessitate active stabilization systems or intricate cavity designs. This makes them highly attractive as they simplify the experimental setup and eliminate the need for complex stabilization mechanisms. In contrast, the design of a cavity can be complex for cavity-enhanced SPDC sources in terms of cavity length, finesse, group velocities, and polarizations of biphotons. Moreover, it is straightforward to switch between doubly- and singly-filtered configurations by simply arranging an optical cavity in different places of the setups without redesigning and rebuilding the experimental setups. In contrast, implementing a similar arrangement in cavity-enhanced SPDC sources poses challenges. This is because the SPDC crystal or waveguide exhibits varying refractive indices for different wavelengths and polarizations of the signal and idler photons. Consequently, the effective cavity lengths differ for the respective resonance conditions, making it challenging to maintain consistent resonance conditions across the entire spectrum.

Compared with cavity-enhanced SPDC sources, although the brightness and photon flux are not enhanced in post-filtered QFCs, they offer a much less demanding flexible configuration for obtaining high-quality biphoton quantum interference fringes,[80,100,153,156] which is fundamental to advanced quantum information-processing tasks. Although there will be unavoidable filtering loss for the generation of high-dimensional QFCs, the robust and stable fiber setups without sophisticated stabilization systems provide an alternate route toward generating large-scale photonic quantum systems for applications such as high-dimensional quantum communications and computations. In addition, for passive filtering QFCs, the FSR, and the cavity round-trip time can be chosen by any user to match the bandwidth of commercial optical bandpass filters, electro-optics phase modulators and the frequency mode spacing of dense wavelength-division multiplexers, enabling single-mode control in the frequency domain. Combining with state-of-the-art SNSPDs with ultra-low timing jitter[56] and mature telecom interferometry technology, the complete and independent time- and frequency-bin control in QFCs is promising for applications ranging from scaling high-dimensional time-frequency entanglement, testing fundamental of quantum non-local nature, to real-world multi-user quantum networks.

HIGH-DIMENSIONAL QUANTUM COMMUNICATIONS WITH QFCs

The intrinsic temporal and spectral multimode structure in mode-locked QFCs is ideally suited for encoding and distributing qubits and qudits with telecom fiber networks. Indeed, for time-bin DoF, the first entanglement distribution experiment was implemented more than two decades ago.[175] Since then, time-bin has become a standard discrete variable to perform entanglement distribution,[231–235] and high-dimensional encoding for QKD.[236–238] In addition, several works implemented the idea of non-local dispersion cancellation,[239,240] using energy-time-entangled biphotons,[170,171,241,242] whose technology is mutually compatible to mature dense wavelength-division-multiplexing-based QKD.[243–247] Based on telecom wavelength-division multiplexing technologies, an integrated QFC has recently been used to generate an energy-time entangled multi-user quantum network.[248] In addition, a frequency entangled qubit state of an on-chip QFC has been distributed through a 24.2-km fiber system.[83] The integrated QFC frequency-bin pairs are each sent through 20-km of standard telecom fiber followed by a 4.2-km dispersion-compensating fiber. These demonstrations show that the frequency entangled states generated in integrated QFCs can be used toward quantum communication tasks.[83,248] In addition, advanced high-dimensional entanglement distribution and frequency-multiplexed large-alphabet QKD in a QFC have been implemented using a singly-filtered scheme[153,158] (Figure 9A). In particular, high-dimensional time-frequency entanglement distribution with five frequency-binned (averaged Franson visibility of 96.70% ± 1.93%, after accidental subtractions) and 16 time-binned non-local interferences (central time-bin has a Franson visibility of 98.85% ± 0.50%, after accidental subtractions) of a singly-filtered QFC at a 10-km distance at near zero-dispersion wavelength has been demonstrated.[153,158] Proof-of-principle frequency-multiplexed time-bin high-dimensional QKD has also been demonstrated using singly- and doubly-filtered QFCs, with a singly-filtered QFC presenting a ≈7.5× improvement on the secret key rate compared with a doubly-filtered QFC under same experimental conditions.[153]

In general, time-bin-based high-dimensional entanglement distribution and QKD are more advantageous than qubit-based QKD for two main reasons. First, the intrinsic dense temporal encoding provides a higher key rate per photon[9,14,250]; second, they exhibit higher tolerance of noise.[10–13] Frequency-multiplexed-based QKD also offers advantages over qubit-based QKD. In frequency-multiplexed QKD, the coincidence rates on the detector side scale linearly with the number of utilized correlated pairs of channels. The primary limitations in this approach are the bandwidth of the SPDC source, the FSR of the cavity, the channel spacing of wavelength-division multiplexers, and the insertion loss associated with these devices.

(F) Real (blue bars) and imaginary (red bars) parts of the measured expectation values for the individual terms of the cluster-state witness operator. The error bars emerge as standard deviations from fits to the experimental data.

(G) A summary table for several recent studies using QFC toward quantum communications and computation. The graph in (A) is reprinted with permission from Cheng et al.,[153] Springer Nature Limited. (B) Reprinted with permission from Seri et al.,[209] APS. (C) Adapted with permission from Niizeki et al.,[249] Springer Nature Limited. (D–F) Adapted from Imany et al.,[87] Springer Nature Limited.

It has been proposed that the simultaneous usage of Franson and conjugate Franson interferometry can enable tighter constraints on the time-frequency covariance matrix of high-dimensional QKD.[127] This unconditional security proof is inspired by the continuous-variable QKD security proofs against Gaussian collective attacks, which use quadrature-component covariance matrices to derive Holevo bounds. It is suitable for qudits due to their ideal infinite Hilbert space. We should point out that Eve's temporal measurement decreases photon coherence, while measuring frequency information increases biphoton correlation time. Therefore, by monitoring the perturbations in Franson and conjugate Franson interference visibilities using dual Bell inequalities, the time-frequency covariance matrix of the energy-time entangled photon pairs can be more accurately constrained. This dual-basis protocol has been proposed to significantly enhance secure key rates, achieving up to 700 bits/s over a transmission distance of 200 km in optical fibers.[127] Furthermore, increasing the temporal pathlength imbalance and amount of frequency shifting ensures a stricter bound, at the expense of higher phase stability requirements for dual-basis interferometry. For comprehensive reviews of high-dimensional QKD, see Xu and co-workers.[177,251–253] Overall, both the time-bin- and frequency-bin-based high-dimensional QKD are rapidly investigated and improved regarding the key figure of merits such as secure key rates versus transmitted distance,[6,7,9] and quantum bit error rates.[5,6,254]

Future quantum communication protocols can be integrated with quantum memory via entanglement swapping and quantum teleportation to realize fully functional quantum repeaters.[213] For instance, the efficient quantum storage of frequency-multiplexes heralded single photons in an atomic frequency comb using a DR-OPO operated at a quantum regime has been demonstrated at 606 nm.[209] By matching atomic frequency comb and QFC in their frequency domain, 15 discrete frequency modes separated by 261 MHz and spanning across 4 GHz are stored[209] (Figure 9B). A DR cavity-enhanced QFC has also been transmitted in a 10-km telecom fiber and then wavelength-converted from 1,514 to 606 nm,[249] for potential integration with efficient visible quantum memory (Figure 9C). More recently, the quantum storage of an integrated QFC using a telecom atomic frequency comb has been demonstrated, achieving record storage time of 1.936 μs.[255] The robustness of multimode operation in both the time and frequency domains within a single spatial mode of QFCs holds potential benefits for quantum satellite applications,[256–259] toward realizing next-generation global-scale quantum networks.

HIGH-DIMENSIONAL QUANTUM COMPUTATION USING QFCs

Besides quantum communication, the qudits also have an advantage in quantum simulation and computation because of a reduction in the number of photons required to span and represent the arbitrary unitary matrix in a d-dimensional system compared with the qubits scenario.[260–264] For example, qudits can implement quantum algorithms using smaller systems and fewer multi-site entangling gates.[263] Recently there has been theoretical proof that universal quantum computation can be realized using only linear optics and SPDC photons in any d+1 dimensional qudit basis.[264]

So far, several studies have successfully demonstrated proof-of-principle quantum computational processing tasks utilizing high-dimensional entanglement in QFCs, including cluster state generations[87,265–270] and stabilizations,[271,272] linear optical quantum computation with passive devices,[273] Bayesian tomography for frequency-bins in QFC,[93] one-way d-level quantum computation via three-level four-partite on-chip QFC,[87] and two-qudit quantum gate operations with fidelities exceeding 90% in the computational basis.[89] More specifically, a controlled increment (CINC) and a SUM two-qudit gate has been utilized to control the multiple frequency-bins using multiple time-bins as target qudit in an integrated QFC.[89] The measured experimental transformation matrix of the CINC and SUM two-qudit gates are confirmed with accidental-subtracted fidelity of 90% ± 1% and 92% ± 1%,[89] respectively. The high-fidelity two-qudit gates, together with arbitrary single-qudit gates, complete a universal set for any quantum computing tasks.

A high-dimensional multipartite quantum state with optimum entanglement witness and highest persistency of entanglement,[274,275] can be generated by transforming a time-frequency hyperentangled state with a controlled phase gate for quantum computation[87] (Figure 9D). Such a controlled phase gate is realized by a fiber Bragg grating array placed in a self-referenced and phase stable loop configuration with synchronized electro-optic phase modulation. The integrated QFC-based cluster state is particularly useful for universal one-way quantum computing because all the information can be written, processed, and readout from the cluster by using only biphoton measurements[275,276] (Figures 9E and 9F). Time-frequency multi-dimensional cluster state from integrated QFCs with measured photon projections on the 81 diagonal elements of the state density matrix (Figure 9E). To confirm genuine multipartite entanglement in cluster state from on-chip QFC, the optimal entanglement witness is performed with an expectation value of 0.28 ± 0.04[87] (Figure 9F). Among the three different types of noise, the d-level cluster state can tolerate 66.6% of incoherent noise with the optimal witness and 37.5% for the measured witness.[87] The computational flow typically goes one way, and feedforward can be implemented between adjacent single-photon detections. Furthermore, the number of time-frequency hyperentangled particles, the number of single photons, as well as the dimensionality of the superposition can be further increased for higher computational performances toward a quantum advantage in the computational tasks.[22,277] This multi-dimensional on-chip QFC and cluster state can thus be generated with significantly higher effective quantum resource rate, toward achieving powerful and fault-tolerant universal quantum computing in CMOS-compatible platforms.[87] In Figure 9G, we provide a summary of recent works that use QFCs for quantum communication and computation tasks. As the methodologies and technologies for high-dimensional entanglement continue to improve, the intrinsic large Hilbert space in temporal and spectral domains of QFCs provide an increasingly elegant way for advanced high-dimensional quantum computing.

Quantum interconnects, which enable the transfer of fragile coherent states between two designated devices, play a crucial role in distributed quantum information processing. These interconnects facilitate the reliable and efficient transfer of qubits and qudits while maintaining essential quantum properties such as superposition and entanglement, fundamental to quantum communication and computing in diverse platforms.[278] There are several types of quantum interconnects, depending on the physical systems used for communications and computation. Examples involve optical quantum interconnects that utilize flying photons in free-space, fiber-based, and chip-scale platforms to transfer quantum information; microwave quantum interconnects with superconducting circuits at cryogenic temperatures; spin-based quantum interconnects that utilize the electrons and spins in solid-state systems; and phononic quantum interconnects via lattice and mechanical vibrations. Hybrid quantum interconnects that combine different quantum technologies are also examined, enabling the faithful transfer of fragile quantum states between different physical segments or DoFs of the overall system. Illustrative examples of hybrid quantum interconnects include, for instance, communication channels,[244,245,252] memories,[199,210,226] frequency conversion and transduction,[279–281] conversion between different encoding schemes or DoFs,[282–285] sensors,[286] simulators,[18,287] and computation[26,60,288] in hybridized larger systems.

Quantifying key parameters in quantum interconnects involves measuring or estimating specific metrics that assess the link performance, efficiency, and reliability. For quantum optical interconnects with recent state-of-the-art QFCs, the time-frequency Hilbert space dimensionality d^N of QFC provides an important role in terms of scalability, providing dense information.[185,289] Furthermore, the QFC multi-photon quantum states have shown advantages in quantum computational processing compared with multi-photon states based on polarization DoF, which only has a two-dimensional subspace.[87] For instance, QFCs from SR-OPO configuration have shown an intrinsic photon-pair rate of 4×10^6, with over 1,000 frequency-bin pairs,[91] and a three-level four-partite cluster state from an integrated QFC has shown orders-of-magnitude improvement in the effective quantum resource rate compared with cluster state based on polarization DoF.[87] Another key parameter in quantum optical interconnects is the fidelity of the photonic quantum state, where QFCs have achieved over 97% quantum state fidelity in Bell-state measurements and in Bayesian tomography,[290] and two-qudit gate fidelities over 90%.[89] In secure-key generation for quantum photonic interconnects, a singly-filtered QFC has presented a total key rate of $\approx$4.7 kbits/s for 5 frequency-bin pairs,[153] with improvements in the source brightness further enhancing the rates. For quantum memories, another indispensable component of quantum optical interconnects, and temporal and spectral multimodes, can be stored and retrieved.[199,210,255] For example, a QFC based on DR-OPO has been stored in an atomic frequency comb quantum memory, with 15 discrete frequency-bins in a storage bandwidth of 4 GHz,[209] and potential higher number of storage modes can be achieved by having broader memory bandwidth, or the narrower FSR of QFCs.

SUMMARY AND OUTLOOK

The energy-time entangled QFCs discussed in this review present a robust and adaptable platform for generating high-dimensional hyperentangled states in a scalable manner. The precise control over the generation of stable, large-scale QFCs is essential but technically demanding. One of the solutions is to develop advanced fabrication techniques for integrated photonics to create robust and stable on-chip QFC sources. The implementation of real-time active feedback and stabilization cavity mechanisms can further help to maintain spectral phase coherence and uniformity in QFCs. Other challenges for QFC sources are noise and loss in the telecom fiber network, which can be mitigated by the developing higher brightness and purity photon-pair sources, and by using low-loss telecom optical components. Moreover, it is possible to use error-correction protocols that are tailored for high-dimensional QFC states.

Advancements in the physics and engineering of the JSI and JTI from SPDC entangled sources enhance the achievable temporal and spectral high-dimensional entanglement in mode-locked QFCs. The current challenge for JTI and JSI measurements of QFC states is that the direct measurement of JTA and JSA is typically difficult to implement in coincidence counting experiments. Continuous development of novel measurement techniques for probing spectral and temporal phases of QFCs are expected to overcome this issue. Furthermore, the employment of advanced quantum machine learning algorithms can help to extract the joint time-frequency information of QFC more efficiently.

High-dimensional entangled states offer a unique framework for manipulating large-scale quantum states within a single spatial mode, leveraging readily available telecommunications components. By synergizing telecom infrastructure with recent rapid developments in integrated quantum photonics, scalable QFCs with low power consumption can be achieved. In high-dimensional time-bin entanglement, the QFC dimensionality is often bounded by the detector jitter and efficiencies, but steady SNSPD developments toward near-unity detection efficiency and low timing jitters have continued to advance the technology envelope. Simultaneously, high-dimensional frequency-bin entanglement is usually bounded by the FSR of the cavity, the operation bandwidth, and the insertion loss of the electro-optic components—these can be scaled by employing smaller FSR cavities, higher bandwidth and lower driving voltage modulators, and integrating lower loss devices. The utilization of on-chip pulse shapers will be helpful in attaining dynamic control of QFC in a lower loss manner.

Regarding the measurement of high-dimensional entangled states, although the full quantum state tomography has limited scalability for higher-dimensional QFCs, advances in high-dimensional time-bin entanglement certification will also solve this problem. For example, the MUB-based witness method may find better scalability toward higher-dimensional QFCs. Moreover, more advanced measurement data-efficient methods, such as Bayesian tomography, have been developed to certify high-dimensional frequency-bin entanglement in QFCs. This can be synergized with improvements on JTI and JSI measurements of QFCs. The future development of frequency-resolved single-photon detectors will also help in the

characterization of high-dimensional frequency-bin entanglement of QFCs.

Highly efficient and deterministic single-photon sources or stochastic photon-pair sources have and will continue to significantly enhance the effectiveness of quantum photonic systems. These sources increase the photon flux, enabling the high-rate generation of higher-dimensional hyperentangled quantum states. Progress in observing and certifying high-dimensional quantum states, leveraging their multimode nature, continue to offer valuable assistance and guidance to experimentalists in fully capitalizing on the capabilities of QFCs. Furthermore, as quantum technologies evolve, we expect that complete and independent time-frequency control of high-dimensional QFCs will be even more accessible in the near future, toward the generation, characterization, and control of arbitrary high-dimensional complex quantum states.

At present, there is a need to bridge the gap between experimental capabilities and practical applications of QFCs. For instance, more focus should be directed to applications where high-dimensional QFCs can provide clear advantages, such as quantum secure QKD, superdense quantum encoding, and multiplexed quantum networks. Collaboration with industrial partners is encouraged to prototype and test QFC-based systems in real-world settings. In addition, while the cluster state or hyperentangled state from QFCs have proven to be resource efficient in quantum computation processing, the scalability of these applications toward large-scale quantum computers can be further enhanced by advancements in QFC generation. Overcoming all of the above-mentioned challenges will require collective efforts across multiple disciplines, including physics, photonics, electronics, computer sciences, and material sciences. Continuous innovation in experimental techniques, theoretical modeling, and technological integration will be critical to unlock the full potential of high-dimensional QFCs, providing new possibilities for high-dimensional encoding schemes, quantum interconnects and memory storage, hardware-efficient quantum computation, sensing, and new protocols in quantum communication networks.

ACKNOWLEDGMENTS

The authors give thanks for useful discussions with J.H. Shapiro and F.N.C. Wong. This work is supported by the Army Research Office (W911NF-21-2-0214) and the National Science Foundation (QuIC-TAQS 2137984 and QII-TAQS 1936375).

AUTHOR CONTRIBUTIONS

K.-C.C., X.C., and C.W.W. initiated the review proposal. K.-C.C. and X.C. made substantial contributions to discussions of the content. K.-C.C., X.C., and M.C.S. researched data for the article. K.-C.C., X.C., M.C.S., and C.W.W. wrote the article and reviewed and/or edited the manuscript before submission.

DECLARATION OF INTERESTS

C.W.W. is an advisory board member for *Newton*.

REFERENCES

1. Vértesi, T., Pironio, S., and Brunner, N. (2010). Closing the detection loophole in Bell experiments using qudits. Phys. Rev. Lett. *104*, 060401. https://doi.org/10.1103/PhysRevLett.104.060401.

2. Shalm, L.K., Meyer-Scott, E., Christensen, B.G., Bierhorst, P., Wayne, M.A., Stevens, M.J., Gerrits, T., Glancy, S., Hamel, D.R., Allman, M.S., et al. (2015). Strong loophole-free test of local realism. Phys. Rev. Lett. *115*, 250402. https://doi.org/10.1103/PhysRevLett.115.250402.

3. Giustina, M., Versteegh, M.A.M., Wengerowsky, S., Handsteiner, J., Hochrainer, A., Phelan, K., Steinlechner, F., Kofler, J., Larsson, J.Å., Abellán, C., et al. (2015). Significant-loophole-free test of Bell's theorem with entangled photons. Phys. Rev. Lett. *115*, 250401. https://doi.org/10.1103/PhysRevLett.115.250401.

4. Vedovato, F., Agnesi, C., Tomasin, M., Avesani, M., Larsson, J.Å., Vallone, G., and Villoresi, P. (2018). Postselection-loophole-free Bell violation with genuine time-bin entanglement. Phys. Rev. Lett. *121*, 190401. https://doi.org/10.1103/PhysRevLett.121.190401.

5. Ali-Khan, I., Broadbent, C.J., and Howell, J.C. (2007). Large-alphabet quantum key distribution using energy-time entangled bipartite states. Phys. Rev. Lett. *98*, 060503. https://doi.org/10.1103/PhysRevLett.98.060503.

6. Zhong, T., Zhou, H., Horansky, R.D., Lee, C., Verma, V.B., Lita, A.E., Restelli, A., Bienfang, J.C., Mirin, R.P., Gerrits, T., et al. (2015). Photon-efficient quantum key distribution using time-energy entanglement with high-dimensional encoding. New J. Phys. *17*, 022002. https://doi.org/10.1088/1367-2630/17/2/022002.

7. Islam, N.T., Lim, C.C.W., Cahall, C., Kim, J., and Gauthier, D.J. (2017). Provably secure and high-rate quantum key distribution with time-bin qudits. Sci. Adv. *3*, e1701491. https://doi.org/10.1126/sciadv.1701491.

8. Epping, M., Kampermann, H., and Bruß, D. (2017). Multi-partite entanglement can speed up quantum key distribution in networks. New J. Phys. *19*, 093012. https://doi.org/10.1088/1367-2630/aa8487.

9. Lee, C., Bunandar, D., Zhang, Z., Steinbrecher, G.R., Ben Dixon, P., Wong, F.N.C., Shapiro, J.H., Hamilton, S.A., and Englund, D. (2019). Large-alphabet encoding for higher-rate quantum key distribution. Opt. Express *27*, 17539–17549. https://doi.org/10.1364/OE.27.017539.

10. Bechmann-Pasquinucci, H., and Peres, A. (2000). Quantum cryptography with 3-state systems. Phys. Rev. Lett. *85*, 3313–3316. https://doi.org/10.1103/PhysRevLett.85.3313.

11. Cerf, N.J., Bourennane, M., Karlsson, A., and Gisin, N. (2002). Security of quantum key distribution using *d*-level systems. Phys. Rev. Lett. *88*, 127902. https://doi.org/10.1103/PhysRevLett.88.127902.

12. Ecker, S., Bouchard, F., Bulla, L., Brandt, F., Kohout, O., Steinlechner, F., Fickler, R., Malik, M., Guryanova, Y., Ursin, R., and Huber, M. (2019). Overcoming noise in entanglement distribution. Phys. Rev. X *9*, 041042. https://doi.org/10.1103/PhysRevX.9.041042.

13. Zhu, F., Tyler, M., Valencia, N.H., Malik, M., and Leach, J. (2021). Is high-dimensional photonic entanglement robust to noise? AVS Quan Sci. *3*, 011401. https://doi.org/10.1116/5.0033889.

14. Doda, M., Huber, M., Murta, G., Pivoluska, M., Plesch, M., and Vlachou, C. (2021). Quantum key distribution overcoming extreme noise: Simultaneous subspace coding using high-dimensional entanglement. Phys. Rev. Appl. *15*, 034003. https://doi.org/10.1103/PhysRevApplied.15.034003.

15. Koczor, B., Endo, S., Jones, T., Matsuzaki, Y., and Benjamin, S.C. (2020). Variational-state quantum metrology. New J. Phys. *22*, 083038. https://doi.org/10.1088/1367-2630/ab965e.

16. Tsang, M., Albarelli, F., and Datta, A. (2020). Quantum semiparametric estimation. Phys. Rev. X *10*, 031023. https://doi.org/10.1103/PhysRevX.10.031023.

17. Lanyon, B.P., Barbieri, M., Almeida, M.P., Jennewein, T., Ralph, T.C., Resch, K.J., Pryde, G.J., O'Brien, J.L., Gilchrist, A., and White, A.G. (2009). Simplifying quantum logic using higher-dimensional Hilbert spaces. Nat. Phys. *5*, 134–140. https://doi.org/10.1038/nphys1150.

18. Georgescu, I.M., Ashhab, S., and Nori, F. (2014). Quantum simulation. Rev. Mod. Phys. *86*, 153–185. https://doi.org/10.1103/RevModPhys.86.153.

19. Wang, D.-S., Stephen, D.T., and Raussendorf, R. (2017). Qudit quantum computation on matrix product states with global symmetry. Phys. Rev. *95*, 032312. https://doi.org/10.1103/PhysRevA.95.032312.

20. McArdle, S., Endo, S., Aspuru-Guzik, A., Benjamin, S.C., and Yuan, X. (2020). Quantum computational chemistry. Rev. Mod. Phys. *92*, 015003. https://doi.org/10.1103/RevModPhys.92.015003.

21. Zhang, J., Pagano, G., Hess, P.W., Kyprianidis, A., Becker, P., Kaplan, H., Gorshkov, A.V., Gong, Z.-X., and Monroe, C. (2017). Observation of a many-body dynamical phase transition with a 53-qubit quantum simulator. Nature *551*, 601–604. https://doi.org/10.1038/nature24654.

22. Arute, F., Arya, K., Babbush, R., Bacon, D., Bardin, J.C., Barends, R., Biswas, R., Boixo, S., Brandao, F.G.S.L., Buell, D.A., et al. (2019). Quantum supremacy using a programmable superconducting processor. Nature *574*, 505–510. https://doi.org/10.1038/s41586-019-1666-5.

23. Arrazola, J.M., Bergholm, V., Brádler, K., Bromley, T.R., Collins, M.J., Dhand, I., Fumagalli, A., Gerrits, T., Goussev, A., Helt, L.G., et al. (2021). Quantum circuits with many photons on a programmable nanophotonic chip. Nature *591*, 54–60. https://doi.org/10.1038/s41586-021-03202-1.

24. Braunstein, S.L., and Van Loock, P. (2005). Quantum information with continuous variables. Rev. Mod. Phys. *77*, 513–577. https://doi.org/10.1103/RevModPhys.77.513.

25. Weedbrook, C., Pirandola, S., García-Patrón, R., Cerf, N.J., Ralph, T.C., Shapiro, J.H., and Lloyd, S. (2012). Gaussian quantum information. Rev. Mod. Phys. *84*, 621–669. https://doi.org/10.1103/RevModPhys.84.621.

26. Kok, P., Munro, W.J., Nemoto, K., Ralph, T.C., Dowling, J.P., and Milburn, G.J. (2007). Linear optical quantum computing with photonic qubits. Rev. Mod. Phys. *79*, 135–174. https://doi.org/10.1103/RevModPhys.79.135.

27. Horodecki, R., Horodecki, P., Horodecki, M., and Horodecki, K. (2009). Quantum entanglement. Rev. Mod. Phys. *81*, 865–942. https://doi.org/10.1103/RevModPhys.81.865.

28. Pan, J.W., Chen, Z.B., Lu, C.Y., Weinfurter, H., Zeilinger, A., and Żukowski, M. (2012). Multiphoton entanglement and interferometry. Rev. Mod. Phys. *84*, 777–838. https://doi.org/10.1103/RevModPhys.84.777.

29. Zhang, K., Liu, S., Chen, Y., Wang, X., and Jing, J. (2022). Optical quantum states based on hot atomic ensembles and their applications. Photon. Insights *1*, R06. https://doi.org/10.3788/PI.2022.R06.

30. Fabre, N., Keller, A., and Milman, P. (2022). Time and frequency as quantum continuous variables. Phys. Rev. *105*, 052429. https://doi.org/10.1103/PhysRevA.105.052429.

31. Yoshikawa, J.I., Yokoyama, S., Kaji, T., Sornphiphatphong, C., Shiozawa, Y., Makino, K., and Furusawa, A. (2016). Invited article: Generation of one-million-mode continuous-variable cluster state by unlimited time-domain multiplexing. APL Photon *1*, 060801. https://doi.org/10.1063/1.4962732.

32. Pinel, O., Jian, P., Medeiros de Araújo, R., Feng, J., Chalopin, B., Fabre, C., and Treps, N. (2012). Generation and characterization of multimode quantum frequency combs. Phys. Rev. Lett. *108*, 083601. https://doi.org/10.1103/PhysRevLett.108.083601.

33. Yokoyama, S., Ukai, R., Armstrong, S.C., Sornphiphatphong, C., Kaji, T., Suzuki, S., Yoshikawa, J.I., Yonezawa, H., Menicucci, N.C., and Furusawa, A. (2013). Ultra-large-scale continuous-variable cluster states multiplexed in the time domain. Nat. Photonics *7*, 982–986. https://doi.org/10.1038/nphoton.2013.287.

34. Chen, M., Menicucci, N.C., and Pfister, O. (2014). Experimental realization of multipartite entanglement of 60 modes of a quantum optical frequency comb. Phys. Rev. Lett. *112*, 120505. https://doi.org/10.1103/PhysRevLett.112.120505.

35. Roslund, J., De Araújo, R.M., Jiang, S., Fabre, C., and Treps, N. (2014). Wavelength-multiplexed quantum networks with ultrafast frequency combs. Nat. Photonics *8*, 109. https://doi.org/10.1038/nphoton.2013.340.

36. Gerke, S., Sperling, J., Vogel, W., Cai, Y., Roslund, J., Treps, N., and Fabre, C. (2015). Full multipartite entanglement of frequency-comb Gaussian states. Phys. Rev. Lett. *114*, 050501. https://doi.org/10.1103/PhysRevLett.114.050501.

37. Cai, Y., Roslund, J., Ferrini, G., Arzani, F., Xu, X., Fabre, C., and Treps, N. (2017). Multimode entanglement in reconfigurable graph states using optical frequency combs. Nat. Commun. *8*, 15645. https://doi.org/10.1038/ncomms15645.

38. Zhu, X., Chang, C.-H., González-Arciniegas, C., Pe'er, A., Higgins, J., and Pfister, O. (2021). Hypercubic cluster states in the phase-modulated quantum optical frequency comb. Optica *8*, 281. https://doi.org/10.1364/OPTICA.411713.

39. Madsen, L.S., Laudenbach, F., Askarani, M.F., Rortais, F., Vincent, T., Bulmer, J.F.F., Miatto, F.M., Neuhaus, L., Helt, L.G., Collins, M.J., et al. (2022). Quantum computational advantage with a programmable photonic processor. Nature *606*, 75–81. https://doi.org/10.1038/s41586-022-04725-x.

40. Larsen, M.V., Guo, X., Breum, C.R., Neergaard-Nielsen, J.S., and Andersen, U.L. (2019). Deterministic generation of a two-dimensional cluster state. Science *366*, 369–372. https://doi.org/10.1126/science.aay4354.

41. Zhao, Y., Okawachi, Y., Jang, J.K., Ji, X., Lipson, M., and Gaeta, A.L. (2020). Near-degenerate quadrature-squeezed vacuum generation on a silicon-nitride chip. Phys. Rev. Lett. *124*, 193601. https://doi.org/10.1103/PhysRevLett.124.193601.

42. Vaidya, V.D., Morrison, B., Helt, L.G., Shahrokshahi, R., Mahler, D.H., Collins, M.J., Tan, K., Lavoie, J., Repingon, A., Menotti, M., et al. (2020). Broadband quadrature-squeezed vacuum and nonclassical photon number correlations from a nanophotonic device. Sci. Adv. *6*, eaba9186. https://doi.org/10.1126/sciadv.aba9186.

43. Yang, Z., Jahanbozorgi, M., Jeong, D., Sun, S., Pfister, O., Lee, H., and Yi, X. (2021). A squeezed quantum microcomb on a chip. Nat. Commun. *12*, 4781. https://doi.org/10.1038/s41467-021-25054-z.

44. Jahanbozorgi, M., Yang, Z., Sun, S., Chen, H., Liu, R., Wang, B., and Yi, X. (2023). Generation of squeezed quantum microcombs with silicon nitride integrated photonic circuits. Optica *10*, 1100. https://doi.org/10.1364/OPTICA.498670.

45. Guidry, M.A., Lukin, D.M., Yang, K.Y., and Vučković, J. (2023). Multimode squeezing in soliton crystal microcombs. Optica *10*, 694. https://doi.org/10.1364/OPTICA.485996.

46. Wang, J., Paesani, S., Ding, Y., Santagati, R., Skrzypczyk, P., Salavrakos, A., Tura, J., Augusiak, R., Mančinska, L., Bacco, D., et al. (2018). Multidimensional quantum entanglement with large-scale integrated optics. Science *360*, 285–291. https://doi.org/10.1126/science.aar7053.

47. Qiang, X., Zhou, X., Wang, J., Wilkes, C.M., Loke, T., O'Gara, S., Kling, L., Marshall, G.D., Santagati, R., Ralph, T.C., et al. (2018). Large-scale silicon quantum photonics implementing arbitrary two-qubit processing. Nat. Photonics *12*, 534–539. https://doi.org/10.1038/s41566-018-0236-y.

48. Adcock, J.C., Vigliar, C., Santagati, R., Silverstone, J.W., and Thompson, M.G. (2019). Programmable four-photon graph states on a silicon chip. Nat. Commun. *10*, 3528. https://doi.org/10.1038/s41467-019-11489-y.

49. Llewellyn, D., Ding, Y., Faruque, I.I., Paesani, S., Bacco, D., Santagati, R., Qian, Y.-J., Li, Y., Xiao, Y.-F., Huber, M., et al. (2019). Chip-to-chip quantum teleportation and multi-photon entanglement in silicon. Nat. Phys. *16*, 148–153. https://doi.org/10.1038/s41567-019-0727-x.

50. Wang, H., He, Y.-M., Chung, T.-H., Hu, H., Yu, Y., Chen, S., Ding, X., Chen, M.-C., Qin, J., Yang, X., et al. (2019). Towards optimal single-photon sources from polarized microcavities. Nat. Photonics *13*, 770–775. https://doi.org/10.1038/s41566-019-0494-3.

51. Uppu, R., Eriksen, H.T., Thyrrestrup, H., Uğurlu, A.D., Wang, Y., Scholz, S., Wieck, A.D., Ludwig, A., Löbl, M.C., Warburton, R.J., et al. (2020).

On-chip deterministic operation of quantum dots in dual-mode waveguides for a plug-and-play single-photon source. Nat. Commun. *11*, 3782. https://doi.org/10.1038/s41467-020-17603-9.

52. Marsili, F., Verma, V.B., Stern, J.A., Harrington, S., Lita, A.E., Gerrits, T., Vayshenker, I., Baek, B., Shaw, M.D., Mirin, R.P., and Nam, S.W. (2013). Detecting single infrared photons with 93% system efficiency. Nat. Photonics *7*, 210–214. https://doi.org/10.1038/nphoton.2013.13.
53. Reddy, D.V., Nerem, R.R., Nam, S.W., Mirin, R.P., and Verma, V.B. (2020). Superconducting nanowire single-photon detectors with 98% system detection efficiency at 1550 nm. Optica *7*, 1649. https://doi.org/10.1364/OPTICA.400751.
54. Chang, J., Los, J.W.N., Tenorio-Pearl, J.O., Noordzij, N., Gourgues, R., Guardiani, A., Zichi, J.R., Pereira, S.F., Urbach, H.P., Zwiller, V., et al. (2021). Detecting telecom single photons with 99.5–2.07+0.5% system detection efficiency and high time resolution. APL Photon *6*, 036114. https://doi.org/10.1063/5.0039772.
55. Hochberg, Y., Charaev, I., Nam, S.W., Verma, V., Colangelo, M., and Berggren, K.K. (2019). Detecting sub-GeV dark matter with superconducting nanowires. Phys. Rev. Lett. *123*, 151802. https://doi.org/10.1103/PhysRevLett.123.151802.
56. Korzh, B., Zhao, Q.-Y., Allmaras, J.P., Frasca, S., Autry, T.M., Bersin, E.A., Beyer, A.D., Briggs, R.M., Bumble, B., Colangelo, M., et al. (2020). Demonstration of sub-3 ps temporal resolution with a superconducting nanowire single-photon detector. Nat. Photonics *14*, 250–255. https://doi.org/10.1038/s41566-020-0589-x.
57. Bouwmeester, D., Pan, J.W., Daniell, M., Weinfurter, H., and Zeilinger, A. (1999). Observation of three-photon Greenberger-Horne-Zeilinger entanglement. Phys. Rev. Lett. *82*, 1345–1349. https://doi.org/10.1103/PhysRevLett.82.1345.
58. Mair, A., Vaziri, A., Weihs, G., and Zeilinger, A. (2001). Entanglement of the orbital angular momentum states of photons. Nature *412*, 313–316. https://doi.org/10.1038/35085529.
59. Vaziri, A., Weihs, G., and Zeilinger, A. (2002). Experimental two-photon, three-dimensional entanglement for quantum communication. Phys. Rev. Lett. *89*, 240401. https://doi.org/10.1103/PhysRevLett.89.240401.
60. Vaziri, A., Pan, J.W., Jennewein, T., Weihs, G., and Zeilinger, A. (2003). Concentration of higher dimensional entanglement: Qutrits of photon orbital angular momentum. Phys. Rev. Lett. *91*, 227902. https://doi.org/10.1103/PhysRevLett.91.227902.
61. Walther, P., Resch, K.J., Rudolph, T., Schenck, E., Weinfurter, H., Vedral, V., Aspelmeyer, M., and Zeilinger, A. (2005). Experimental one-way quantum computing. Nature *434*, 169–176. https://doi.org/10.1038/nature03347.
62. Vallone, G., Donati, G., Ceccarelli, R., and Mataloni, P. (2010). Six-qubit two-photon hyperentangled cluster states: Characterization and application to quantum computation. Phys. Rev. *81*, 052301. https://doi.org/10.1103/PhysRevA.81.052301.
63. Dada, A.C., Leach, J., Buller, G.S., Padgett, M.J., and Andersson, E. (2011). Experimental high-dimensional two-photon entanglement and violations of generalized Bell inequalities. Nat. Phys. *7*, 677–680. https://doi.org/10.1038/nphys1996.
64. Romero, J., Giovannini, D., Franke-Arnold, S., Barnett, S.M., and Padgett, M.J. (2012). Increasing the dimension in high-dimensional two-photon orbital angular momentum entanglement. Phys. Rev. *86*, 012334. https://doi.org/10.1103/PhysRevA.86.012334.
65. Krenn, M., Huber, M., Fickler, R., Lapkiewicz, R., Ramelow, S., and Zeilinger, A. (2014). Generation and confirmation of a (100×100)-dimensional entangled quantum system. Proc. Natl. Acad. Sci. USA *111*, 6243–6247. https://doi.org/10.1073/pnas.1402365111.
66. Willner, A.E., Huang, H., Yan, Y., Ren, Y., Ahmed, N., Xie, G., Bao, C., Li, L., Cao, Y., Zhao, Z., et al. (2015). Optical communications using orbital angular momentum beams. Adv. Opt Photon *7*, 66. https://doi.org/10.1364/AOP.7.000066.
67. Malik, M., Erhard, M., Huber, M., Krenn, M., Fickler, R., and Zeilinger, A. (2016). Multi-photon entanglement in high dimensions. Nat. Photonics *10*, 248–252. https://doi.org/10.1038/nphoton.2016.12.
68. Krenn, M., Handsteiner, J., Fink, M., Fickler, R., Ursin, R., Malik, M., and Zeilinger, A. (2016). Twisted light transmission over 143 km. Proc. Natl. Acad. Sci. USA *113*, 13648–13653. https://doi.org/10.1073/pnas.1612023113.
69. Babazadeh, A., Erhard, M., Wang, F., Malik, M., Nouroozi, R., Krenn, M., and Zeilinger, A. (2017). High-dimensional single-photon quantum gates: Concepts and experiments. Phys. Rev. Lett. *119*, 180510. https://doi.org/10.1103/PhysRevLett.119.180510.
70. Wang, F., Erhard, M., Babazadeh, A., Malik, M., Krenn, M., and Zeilinger, A. (2017). Generation of the complete four-dimensional Bell basis. Optica *4*, 1462. https://doi.org/10.1364/OPTICA.4.001462.
71. Krenn, M., Hochrainer, A., Lahiri, M., and Zeilinger, A. (2017). Entanglement by path identity. Phys. Rev. Lett. *118*, 080401. https://doi.org/10.1103/PhysRevLett.118.080401.
72. Erhard, M., Fickler, R., Krenn, M., and Zeilinger, A. (2018). Twisted photons: New quantum perspectives in high dimensions. Light Sci. Appl. *7*, 17146. https://doi.org/10.1038/lsa.2017.146.
73. Cozzolino, D., Bacco, D., Da Lio, B., Ingerslev, K., Ding, Y., Dalgaard, K., Kristensen, P., Galili, M., Rottwitt, K., Ramachandran, S., and Oxenløwe, L.K. (2019). Orbital angular momentum states enabling fiber-based high-dimensional quantum communication. Phys. Rev., A. *11*, 064058. https://doi.org/10.1103/PhysRevApplied.11.064058.
74. Brandt, F., Hiekkamäki, M., Bouchard, F., Huber, M., and Fickler, R. (2020). High-dimensional quantum gates using full-field spatial modes of photons. Optica *7*, 98. https://doi.org/10.1364/OPTICA.375875.
75. Kysela, J., Erhard, M., Hochrainer, A., Krenn, M., and Zeilinger, A. (2020). Path identity as a source of high-dimensional entanglement. Proc. Natl. Acad. Sci. USA *117*, 26118–26122. https://doi.org/10.1073/pnas.2011405117.
76. Ou, Z.Y., and Lu, Y.J. (1999). Cavity enhanced spontaneous parametric down-conversion for the prolongation of correlation time between conjugate photons. Phys. Rev. Lett. *83*, 2556–2559. https://doi.org/10.1103/PhysRevLett.83.2556.
77. Lu, Y.J., Campbell, R.L., and Ou, Z.Y. (2003). Mode-locked two-photon states. Phys. Rev. Lett. *91*, 163602. https://doi.org/10.1103/PhysRevLett.91.163602.
78. Reimer, C., Caspani, L., Clerici, M., Ferrera, M., Kues, M., Peccianti, M., Pasquazi, A., Razzari, L., Little, B.E., Chu, S.T., et al. (2014). Integrated frequency comb source of heralded single photons. Opt. Express *22*, 6535–6546. https://doi.org/10.1364/OE.22.006535.
79. Reimer, C., Kues, M., Caspani, L., Wetzel, B., Roztocki, P., Clerici, M., Jestin, Y., Ferrera, M., Peccianti, M., Pasquazi, A., et al. (2015). Cross-polarized photon-pair generation and bi-chromatically pumped optical parametric oscillation on a chip. Nat. Commun. *6*, 8236. https://doi.org/10.1038/ncomms9236.
80. Xie, Z., Zhong, T., Shrestha, S., Xu, X., Liang, J., Gong, Y.X., Bienfang, J.C., Restelli, A., Shapiro, J.H., Wong, F.N.C., and Wei Wong, C. (2015). Harnessing high-dimensional hyperentanglement through a biphoton frequency comb. Nat. Photonics *9*, 536–542. https://doi.org/10.1038/nphoton.2015.110.
81. Reimer, C., Kues, M., Roztocki, P., Wetzel, B., Grazioso, F., Little, B.E., Chu, S.T., Johnston, T., Bromberg, Y., Caspani, L., et al. (2016). Generation of multiphoton entangled quantum states by means of integrated frequency combs. Science *351*, 1176–1180. https://doi.org/10.1126/science.aad8532.
82. Jaramillo-Villegas, J.A., Imany, P., Odele, O.D., Leaird, D.E., Ou, Z.-Y., Qi, M., and Weiner, A.M. (2017). Persistent energy-time entanglement covering multiple resonances of an on-chip biphoton frequency comb. Optica *4*, 655. https://doi.org/10.1364/OPTICA.4.000655.

83. Kues, M., Reimer, C., Roztocki, P., Cortés, L.R., Sciara, S., Wetzel, B., Zhang, Y., Cino, A., Chu, S.T., Little, B.E., et al. (2017). On-chip generation of high-dimensional entangled quantum states and their coherent control. Nature *546*, 622–626. https://doi.org/10.1038/nature22986.

84. Mahmudlu, H., Johanning, R., van Rees, A., Khodadad Kashi, A., Epping, J.P., Haldar, R., Boller, K.-J., and Kues, M. (2023). Fully on-chip photonic turnkey quantum source for entangled qubit/qudit state generation. Nat. Photonics *17*, 518–524. https://doi.org/10.1038/s41566-023-01193-1.

85. Imany, P., Jaramillo-Villegas, J.A., Odele, O.D., Han, K., Leaird, D.E., Lukens, J.M., Lougovski, P., Qi, M., and Weiner, A.M. (2018). 50-GHz-spaced comb of high-dimensional frequency-bin entangled photons from an on-chip silicon nitride microresonator. Opt. Express *26*, 1825–1840. https://doi.org/10.1364/OE.26.001825.

86. Lu, H.-H., Lukens, J.M., Peters, N.A., Williams, B.P., Weiner, A.M., and Lougovski, P. (2018). Quantum interference and correlation control of frequency-bin qubits. Optica *5*, 1455. https://doi.org/10.1364/OPTICA.5.001455.

87. Reimer, C., Sciara, S., Roztocki, P., Islam, M., Romero Cortés, L., Zhang, Y., Fischer, B., Loranger, S., Kashyap, R., Cino, A., et al. (2019). High-dimensional one-way quantum processing implemented on *d*-level cluster states. Nat. Phys. *15*, 148–153. https://doi.org/10.1038/s41567-018-0347-x.

88. Lu, H.-H., Lukens, J.M., Williams, B.P., Imany, P., Peters, N.A., Weiner, A.M., and Lougovski, P. (2019). A controlled-NOT gate for frequency-bin qubits. npj Quan. Inf. *5*, 24. https://doi.org/10.1038/s41534-019-0137-z.

89. Imany, P., Jaramillo-Villegas, J.A., Alshaykh, M.S., Lukens, J.M., Odele, O.D., Moore, A.J., Leaird, D.E., Qi, M., and Weiner, A.M. (2019). High-dimensional optical quantum logic in large operational spaces. npj Quan. Inf. *5*, 59. https://doi.org/10.1038/s41534-019-0173-8.

90. Lingaraju, N.B., Lu, H.-H., Seshadri, S., Imany, P., Leaird, D.E., Lukens, J.M., and Weiner, A.M. (2019). Quantum frequency combs and Hong-Ou-Mandel interferometry: The role of spectral phase coherence. Opt. Express *27*, 38683–38697. https://doi.org/10.1364/OE.379749.

91. Ikuta, R., Tani, R., Ishizaki, M., Miki, S., Yabuno, M., Terai, H., Imoto, N., and Yamamoto, T. (2019). Frequency-multiplexed photon pairs over 1000 modes from a quadratic nonlinear optical waveguide resonator with a singly resonant configuration. Phys. Rev. Lett. *123*, 193603. https://doi.org/10.1103/PhysRevLett.123.193603.

92. Zhang, Y., Kues, M., Roztocki, P., Reimer, C., Fischer, B., MacLellan, B., Bisianov, A., Peschel, U., Little, B.E., Chu, S.T., et al. (2020). Induced photon correlations through the overlap of two four-wave mixing processes in integrated cavities. Laser Photon. Rev. *14*, 2000128. https://doi.org/10.1002/lpor.202000128.

93. Lu, H.-H., Myilswamy, K.V., Bennink, R.S., Seshadri, S., Alshaykh, M.S., Liu, J., Kippenberg, T.J., Leaird, D.E., Weiner, A.M., and Lukens, J.M. (2022). Bayesian tomography of high-dimensional on-chip biphoton frequency combs with randomized measurements. Nat. Commun. *13*, 4338. https://doi.org/10.1038/s41467-022-31639-z.

94. Hu, Y., Reimer, C., Shams-Ansari, A., Zhang, M., and Loncar, M. (2020). Realization of high-dimensional frequency crystals in electro-optic microcombs. Optica *7*, 1189–1196. https://doi.org/10.1364/OPTICA.395114.

95. Imany, P., Lingaraju, N.B., Alshaykh, M.S., Leaird, D.E., and Weiner, A.M. (2020). Probing quantum walks through coherent control of high-dimensionally entangled photons. Sci. Adv. *6*, eaba8066. https://doi.org/10.1126/sciadv.aba8066.

96. Joshi, C., Farsi, A., Dutt, A., Kim, B.Y., Ji, X., Zhao, Y., Bishop, A.M., Lipson, M., and Gaeta, A.L. (2020). Frequency-domain quantum interference with correlated photons from an integrated microresonator. Phys. Rev. Lett. *124*, 143601. https://doi.org/10.1103/PhysRevLett.124.143601.

97. Fabre, N., Maltese, G., Appas, F., Felicetti, S., Ketterer, A., Keller, A., Coudreau, T., Baboux, F., Amanti, M.I., Ducci, S., and Milman, P. (2020). Generation of a time-frequency grid state with integrated biphoton frequency combs. Phys. Rev. *102*, 012607. https://doi.org/10.1103/PhysRevA.102.012607.

98. Maltese, G., Amanti, M.I., Appas, F., Sinnl, G., Lemaître, A., Milman, P., Baboux, F., and Ducci, S. (2020). Generation and symmetry control of quantum frequency combs. npj Quan. Inf. *6*, 13. https://doi.org/10.1038/s41534-019-0237-9.

99. Lingaraju, N.B., Lu, H.-H., Seshadri, S., Leaird, D.E., Weiner, A.M., and Lukens, J.M. (2021). Adaptive bandwidth management for entanglement distribution in quantum networks. Optica *8*, 329–335. https://doi.org/10.1364/OPTICA.413657.

100. Chang, K.-C., Cheng, X., Sarihan, M.C., Vinod, A.K., Lee, Y.S., Zhong, T., Gong, Y.-X., Xie, Z., Shapiro, J.H., Wong, F.N.C., and Wong, C.W. (2021). Hilbert space dimensionality in a biphoton frequency comb: entanglement formation and Schmidt mode decomposition. npj Quan. Inf. *7*, 48. https://doi.org/10.1038/s41534-021-00388-0.

101. Yamazaki, T., Ikuta, R., Kobayashi, T., Miki, S., China, F., Terai, H., Imoto, N., and Yamamoto, T. (2022). Massive-mode polarization entangled biphoton frequency comb. Sci. Rep. *12*, 8964. https://doi.org/10.1038/s41598-022-12691-7.

102. Wen, W., Yan, W., Lu, C., Lu, L., Wu, X., Lu, Y., Zhu, S., and Ma, X.S. (2023). Polarization-entangled quantum frequency comb from a silicon nitride microring resonator. Phys. Rev. Appl. *20*, 064032. https://doi.org/10.1103/PhysRevApplied.20.064032.

103. Lu, L., Xia, L., Chen, Z., Chen, L., Yu, T., Tao, T., Ma, W., Pan, Y., Cai, X., Lu, Y., et al. (2020). Three-dimensional entanglement on a silicon chip. npj Quan. Inf. *6*, 30. https://doi.org/10.1038/s41534-020-0260-x.

104. Slussarenko, S., and Pryde, G.J. (2019). Photonic quantum information processing: A concise review. Appl. Phys. Rev. *6*, 041303. https://doi.org/10.1063/1.5115814.

105. Xavier, G.B., and Lima, G. (2020). Quantum information processing with space-division multiplexing optical fibres. Commun. Phys. *3*, 9. https://doi.org/10.1038/s42005-019-0269-7.

106. Wang, J., Sciarrino, F., Laing, A., and Thompson, M.G. (2020). Integrated photonic quantum technologies. Nat. Photonics *14*, 273–284. https://doi.org/10.1038/s41566-019-0532-1.

107. Erhard, M., Krenn, M., and Zeilinger, A. (2020). Advances in high-dimensional quantum entanglement. Nat. Rev. Phys. *2*, 365–381. https://doi.org/10.1038/s42254-020-0193-5.

108. Kues, M., Reimer, C., Lukens, J.M., Munro, W.J., Weiner, A.M., Moss, D.J., and Morandotti, R. (2019). Quantum optical microcombs. Nat. Photonics *13*, 170–179. https://doi.org/10.1038/s41566-019-0363-0.

109. Weiner, A. (2009). Ultrafast Optics, *72* (John Wiley & Sons).

110. Shapiro, J.H. (2002). Coincidence dips and revivals from a Type-II optical parametric amplifier. In Technical Digest of Topical Conference on Nonlinear Optics (Optica Publishing Group), paper FC7-1, Maui, HI. https://doi.org/10.1364/NLO.2002.FC7.

111. Rambach, M., Lau, W.Y.S., Laibacher, S., Tamma, V., White, A.G., and Weinhold, T.J. (2018). Hectometer revivals of quantum interference. Phys. Rev. Lett. *121*, 093603. https://doi.org/10.1103/PhysRevLett.121.093603.

112. Jin, R.B., Shimizu, R., Fujiwara, M., Takeoka, M., Wakabayashi, R., Yamashita, T., Miki, S., Terai, H., Gerrits, T., and Sasaki, M. (2016). Simple method of generating and distributing frequency-entangled qudits. Quantum Sci. Technol. *1*, 015004. https://doi.org/10.1088/2058-9565/1/1/015004.

113. Jin, R.B., Zeng, Z.Q., Xu, D., Yuan, C.Z., Li, B.H., Wang, Y., Shimizu, R., Takeoka, M., Fujiwara, M., Sasaki, M., and Lu, P.X. (2024). Spectrally resolved Franson interference. Sci. China Phys. Mech. Astron. *67*, 250312. https://doi.org/10.1007/s11433-023-2326-7.

114. Morrison, C.L., Graffitti, F., Barrow, P., Pickston, A., Ho, J., and Fedrizzi, A. (2022). Frequency-bin entanglement from domain-engineered down-conversion. APL Photon *7*, 066101. https://doi.org/10.1063/5.0089313.

115. Shukhin, A., Hurvitz, I., Trajtenberg-Mills, S., Arie, A., and Eisenberg, H. (2024). Two-dimensional control of a biphoton joint spectrum. Opt. Express *32*, 10158–10174. https://doi.org/10.1364/OE.510497.

116. Scholz, M., Koch, L., Ullmann, R., and Benson, O. (2009). Single-mode operation of a high-brightness narrow-band single-photon source. Appl. Phys. Lett. *94*, 201105. https://doi.org/10.1063/1.3139768.

117. Luo, K.H., Ansari, V., Massaro, M., Santandrea, M., Eigner, C., Ricken, R., Herrmann, H., and Silberhorn, C. (2020). Counter-propagating photon pair generation in a nonlinear waveguide. Opt. Express *28*, 3215–3225. https://doi.org/10.1364/OE.378789.

118. Pe'Er, A., Dayan, B., Friesem, A.A., and Silberberg, Y. (2005). Temporal shaping of entangled photons. Phys. Rev. Lett. *94*, 073601. https://doi.org/10.1103/PhysRevLett.94.073601.

119. Kuzucu, O., Wong, F.N.C., Kurimura, S., and Tovstonog, S. (2008). Joint temporal density measurements for two-photon state characterization. Phys. Rev. Lett. *101*, 153602. https://doi.org/10.1103/PhysRevLett.101.153602.

120. MacLean, J.-P.W., Donohue, J.M., and Resch, K.J. (2018). Direct characterization of ultrafast energy-time entangled photon pairs. Phys. Rev. Lett. *120*, 053601. https://doi.org/10.1103/PhysRevLett.120.053601.

121. Mittal, S., Orre, V.V., Restelli, A., Salem, R., Goldschmidt, E.A., and Hafezi, M. (2017). Temporal and spectral manipulations of correlated photons using a time lens. Phys. Rev. *96*, 043807. https://doi.org/10.1103/PhysRevA.96.043807.

122. Beduini, F.A., Zielińska, J.A., Lucivero, V.G., de Icaza Astiz, Y.A., and Mitchell, M.W. (2014). Interferometric measurement of the biphoton wave function. Phys. Rev. Lett. *113*, 183602. https://doi.org/10.1103/PhysRevLett.113.183602.

123. Davis, A.O.C., Thiel, V., Karpiński, M., and Smith, B.J. (2018). Measuring the single-photon temporal-spectral wave function. Phys. Rev. Lett. *121*, 083602. https://doi.org/10.1103/PhysRevLett.121.083602.

124. Davis, A.O.C., Thiel, V., and Smith, B.J. (2020). Measuring the quantum state of a photon pair entangled in frequency and time. Optica *7*, 1317. https://doi.org/10.1364/OPTICA.396933.

125. Liu, Y.C., Guo, D.J., Yang, R., Sun, C.W., Duan, J.C., Gong, Y.X., Xie, Z., and Zhu, S.N. (2021). Narrowband photonic quantum entanglement with counterpropagating domain engineering. Photon. Res. *9*, 1998. https://doi.org/10.1364/PRJ.413075.

126. Chen, P., Shu, C., Guo, X., Loy, M.M.T., and Du, S. (2015). Measuring the biphoton temporal wave function with polarization-dependent and time-resolved two-photon interference. Phys. Rev. Lett. *114*, 010401. https://doi.org/10.1103/PhysRevLett.114.010401.

127. Zhang, Z., Mower, J., Englund, D., Wong, F.N.C., and Shapiro, J.H. (2014). Unconditional security of time-energy entanglement quantum key distribution using dual-basis interferometry. Phys. Rev. Lett. *112*, 120506. https://doi.org/10.1103/PhysRevLett.112.120506.

128. Chen, C., Shapiro, J.H., and Wong, F.N.C. (2021). Experimental demonstration of conjugate-Franson interferometry. Phys. Rev. Lett. *127*, 093603. https://doi.org/10.1103/PhysRevLett.127.093603.

129. Chen, C., Bo, C., Niu, M.Y., Xu, F., Zhang, Z., Shapiro, J.H., and Wong, F.N.C. (2017). Efficient generation and characterization of spectrally factorable biphotons. Opt. Express *25*, 7300–7312. https://doi.org/10.1364/OE.25.007300.

130. Donohue, J.M., Mastrovich, M., and Resch, K.J. (2016). Spectrally engineering photonic entanglement with a time lens. Phys. Rev. Lett. *117*, 243602. https://doi.org/10.1103/PhysRevLett.117.243602.

131. Averchenko, V., Sych, D., Marquardt, C., and Leuchs, G. (2020). Efficient generation of temporally shaped photons using non-local spectral filtering. Phys. Rev. *101*, 013808. https://doi.org/10.1103/PhysRevA.101.013808.

132. Gianani, I., Sbroscia, M., and Barbieri, M. (2020). Measuring the time-frequency properties of photon pairs: A short review. AVS Quan. Sci. *2*, 011701. https://doi.org/10.1116/1.5136340.

133. Olislager, L., Cussey, J., Nguyen, A.T., Emplit, P., Massar, S., Merolla, J.M., and Huy, K.P. (2010). Frequency-bin entangled photons. Phys. Rev. *82*, 013804. https://doi.org/10.1103/PhysRevA.82.013804.

134. Mosley, P.J., Lundeen, J.S., Smith, B.J., Wasylczyk, P., U'Ren, A.B., Silberhorn, C., and Walmsley, I.A. (2008). Heralded generation of ultrafast single photons in pure quantum states. Phys. Rev. Lett. *100*, 133601. https://doi.org/10.1103/PhysRevLett.100.133601.

135. Gerrits, T., Stevens, M.J., Baek, B., Calkins, B., Lita, A., Glancy, S., Knill, E., Nam, S.W., Mirin, R.P., Hadfield, R.H., et al. (2011). Generation of degenerate, factorizable, pulsed squeezed light at telecom wavelengths. Opt. Express *19*, 24434–24447. https://doi.org/10.1364/OE.19.024434.

136. Bell, B.A., Triginer Garces, G., and Walmsley, I.A. (2020). Diagnosing phase correlations in the joint spectrum of parametric downconversion using multi-photon emission. Opt. Express *28*, 34246–34254. https://doi.org/10.1364/OE.401258.

137. Avenhaus, M., Eckstein, A., Mosley, P.J., and Silberhorn, C. (2009). Fiber-assisted single-photon spectrograph. Opt. Lett. *34*, 2873–2875. https://doi.org/10.1364/OL.34.002873.

138. Harder, G., Ansari, V., Brecht, B., Dirmeier, T., Marquardt, C., and Silberhorn, C. (2013). An optimized photon pair source for quantum circuits. Opt. Express *21*, 13975–13985. https://doi.org/10.1364/OE.21.013975.

139. Gerrits, T., Marsili, F., Verma, V.B., Shalm, L.K., Shaw, M., Mirin, R.P., and Nam, S.W. (2015). Spectral correlation measurements at the Hong-Ou-Mandel interference dip. Phys. Rev. *91*, 013830. https://doi.org/10.1103/PhysRevA.91.013830.

140. Weston, M.M., Chrzanowski, H.M., Wollmann, S., Boston, A., Ho, J., Shalm, L.K., Verma, V.B., Allman, M.S., Nam, S.W., Patel, R.B., et al. (2016). Efficient and pure femtosecond-pulse-length source of polarization-entangled photons. Opt. Express *24*, 10869–10879. https://doi.org/10.1364/OE.24.010869.

141. Orre, V.V., Goldschmidt, E.A., Deshpande, A., Gorshkov, A.V., Tamma, V., Hafezi, M., and Mittal, S. (2019). Interference of temporally distinguishable photons using frequency-resolved detection. Phys. Rev. Lett. *123*, 123603. https://doi.org/10.1103/PhysRevLett.123.123603.

142. Chen, C., Heyes, J.E., Hong, K.H., Niu, M.Y., Lita, A.E., Gerrits, T., Nam, S.W., Shapiro, J.H., and Wong, F.N.C. (2019). Indistinguishable single-mode photons from spectrally engineered biphotons. Opt. Express *27*, 11626–11634. https://doi.org/10.1364/OE.27.011626.

143. Graffitti, F., Barrow, P., Pickston, A., Brańczyk, A.M., and Fedrizzi, A. (2020). Direct generation of tailored pulse-mode entanglement. Phys. Rev. Lett. *124*, 053603. https://doi.org/10.1103/PhysRevLett.124.053603.

144. Pickston, A., Graffitti, F., Barrow, P., Morrison, C.L., Ho, J., Brańczyk, A.M., and Fedrizzi, A. (2021). Optimised domain-engineered crystals for pure telecom photon sources. Opt. Express *29*, 6991–7002. https://doi.org/10.1364/OE.416843.

145. Tischler, N., Büse, A., Helt, L.G., Juan, M.L., Piro, N., Ghosh, J., Steel, M.J., and Molina-Terriza, G. (2015). Measurement and shaping of biphoton spectral wave functions. Phys. Rev. Lett. *115*, 193602. https://doi.org/10.1103/PhysRevLett.115.193602.

146. Jizan, I., Bell, B., Helt, L.G., Bedoya, A.C., Xiong, C., and Eggleton, B.J. (2016). Phase-sensitive tomography of the joint spectral amplitude of photon pair sources. Opt. Lett. *41*, 4803–4806. https://doi.org/10.1364/OL.41.004803.

147. MacLean, J.-P.W., Schwarz, S., and Resch, K.J. (2019). Reconstructing ultrafast energy-time-entangled two-photon pulses. Phys. Rev. *100*, 033834. https://doi.org/10.1103/PhysRevA.100.033834.

148. Triginer, G., Vidrighin, M.D., Quesada, N., Eckstein, A., Moore, M., Kolthammer, W.S., Sipe, J.E., and Walmsley, I.A. (2020). Understanding high-gain twin-beam sources using cascaded stimulated emission. Phys. Rev. X *10*, 031063. https://doi.org/10.1103/PhysRevX.10.031063.

149. Gianani, I. (2019). Robust spectral phase reconstruction of time-frequency entangled bi-photon states. Phys. Rev. Res. *1*, 033165. https://doi.org/10.1103/PhysRevRes.1.033165.

150. Javid, U.A., Ling, J., Staffa, J., Li, M., He, Y., and Lin, Q. (2021). Ultra-broadband entangled photons on a nanophotonic chip. Phys. Rev. Lett. *127*, 183601. https://doi.org/10.1103/PhysRevLett.127.183601.

151. Okoth, C., Cavanna, A., Santiago-Cruz, T., and Chekhova, M.V. (2019). Microscale generation of entangled photons without momentum conservation. Phys. Rev. Lett. *123*, 263602. https://doi.org/10.1103/PhysRevLett.123.263602.

152. Franson, J.D. (1989). Bell inequality for position and time. Phys. Rev. Lett. *62*, 2205–2208. https://doi.org/10.1103/PhysRevLett.62.2205.

153. Cheng, X., Chang, K.-C., Sarihan, M.C., Mueller, A., Spiropulu, M., Shaw, M.D., Korzh, B., Faraon, A., Wong, F.N.C., Shapiro, J.H., and Wong, C.W. (2023). High-dimensional time-frequency entanglement in a singly-filtered biphoton frequency comb. Commun. Phys. *6*, 278. https://doi.org/10.1038/s42005-023-01370-2.

154. Scholz, M., Koch, L., and Benson, O. (2009). Statistics of narrow-band single photons for quantum memories generated by ultrabright cavity-enhanced parametric down-conversion. Phys. Rev. Lett. *102*, 063603. https://doi.org/10.1103/PhysRevLett.102.063603.

155. Martin, A., Guerreiro, T., Tiranov, A., Designolle, S., Fröwis, F., Brunner, N., Huber, M., and Gisin, N. (2017). Quantifying photonic high-dimensional entanglement. Phys. Rev. Lett. *118*, 110501. https://doi.org/10.1103/PhysRevLett.118.110501.

156. Chang, K.-C., Cheng, X., Sarihan, M.C., Wong, C.W., Mueller, A., Spiropulu, M., Shaw, M.D., Korzh, B., Huber, M., and Wong, C.W. (2023). Towards optimum Franson interference recurrence in mode-locked singly-filtered biphoton frequency combs. Photon. Res. *11*, 1175. https://doi.org/10.1364/PRJ.483570.

157. Chang, K.-C., Cheng, X., Sarihan, M.C., and Wong, C.W. (2024). Time-reversible and fully time-resolved ultranarrow-band biphoton frequency combs. APL Quantum *1*, 016106. https://doi.org/10.1063/5.0180543.

158. Chang, K.-C., Cheng, X., Sarihan, M.C., Wong, F.N.C., Shapiro, J.H., and Wong, C.W. (2021). High-dimensional energy-time entanglement distribution via a biphoton frequency comb. In *Conference on Lasers and Electro-Optics*, OSA Technical Digest (Optical Society of America). https://doi.org/10.1364/CLEO_QELS.2021.FF1A.7.

159. Brendel, J., Gisin, N., Tittel, W., and Zbinden, H. (1999). Pulsed energy-time entangled twin-photon source for quantum communication. Phys. Rev. Lett. *82*, 2594–2597. https://doi.org/10.1103/PhysRevLett.82.2594.

160. Thew, R.T., Tanzilli, S., Tittel, W., Zbinden, H., and Gisin, N. (2002). Experimental investigation of the robustness of partially entangled qubits over 11 km. Phys. Rev. *66*, 062304. https://doi.org/10.1103/PhysRevA.66.062304.

161. De Riedmatten, H., Marcikic, I., Scarani, V., Tittel, W., Zbinden, H., and Gisin, N. (2004). Tailoring photonic entanglement in high-dimensional Hilbert spaces. Phys. Rev. *69*, 050304. https://doi.org/10.1103/PhysRevA.69.050304.

162. Ikuta, T., and Takesue, H. (2017). Implementation of quantum state tomography for time-bin qudits. New J. Phys. *19*, 013039. https://doi.org/10.1088/1367-2630/aa5571.

163. Brougham, T., Barnett, S.M., McCusker, K.T., Kwiat, P.G., and Gauthier, D.J. (2013). Security of high-dimensional quantum key distribution protocols using Franson interferometers. J. Phys. B Atom. Mol. Opt. Phys. *46*, 104010. https://doi.org/10.1088/0953-4075/46/10/104010.

164. Friis, N., Vitagliano, G., Malik, M., and Huber, M. (2018). Entanglement certification from theory to experiment. Nat. Rev. Phys. *1*, 72–87. https://doi.org/10.1038/s42254-018-0003-5.

165. Giovannini, D., Romero, J., Leach, J., Dudley, A., Forbes, A., and Padgett, M.J. (2013). Characterization of high-dimensional entangled systems via mutually unbiased measurements. Phys. Rev. Lett. *110*, 143601. https://doi.org/10.1103/PhysRevLett.110.143601.

166. Coles, P.J., Berta, M., Tomamichel, M., and Wehner, S. (2017). Entropic uncertainty relations and their applications. Rev. Mod. Phys. *89*, 015002. https://doi.org/10.1103/RevModPhys.89.015002.

167. Ding, Y., Bacco, D., Dalgaard, K., Cai, X., Zhou, X., Rottwitt, K., and Oxenløwe, L.K. (2017). High-dimensional quantum key distribution based on multicore fiber using silicon photonic integrated circuits. npj Quan. Inf. *3*, 25. https://doi.org/10.1038/s41534-017-0026-2.

168. Bavaresco, J., Valencia, N.H., Klöckl, C., Pivoluska, M., Erker, P., Friis, N., Malik, M., and Huber, M. (2018). Measurements in two bases are sufficient for certifying high-dimensional entanglement. Nat. Phys. *14*, 1032. https://doi.org/10.1038/s41567-018-0203-z.

169. Chang, K.-C., Sarihan, M.C., Cheng, X., Erker, P., Mueller, A., Spiropulu, M., Shaw, M.D., Korzh, B., Huber, M., and Wong, C.W. (2023). Experimental high-dimensional entanglement certification and quantum steering with time-energy measurements. Preprint at arXiv. https://arxiv.org/abs/2310.20694.

170. Mower, J., Zhang, Z., Desjardins, P., Lee, C., Shapiro, J.H., and Englund, D. (2013). High-dimensional quantum key distribution using dispersive optics. Phys. Rev. *87*, 062322. https://doi.org/10.1103/PhysRevA.87.062322.

171. Lee, C., Zhang, Z., Steinbrecher, G.R., Zhou, H., Mower, J., Zhong, T., Wang, L., Hu, X., Horansky, R.D., Verma, V.B., et al. (2014). Entanglement-based quantum communication secured by non-local dispersion cancellation. Phys. Rev. *90*, 062331. https://doi.org/10.1103/PhysRevA.90.062331.

172. Ikuta, T., Akibue, S., Yonezu, Y., Honjo, T., Takesue, H., and Inoue, K. (2022). Scalable implementation of (d+1) mutually unbiased bases for d-dimensional quantum key distribution. Phys. Rev. Res. *4*, L042007. https://doi.org/10.1103/PhysRevRes.4.L042007.

173. Lukens, J.M., Islam, N.T., Lim, C.C.W., and Gauthier, D.J. (2018). Reconfigurable generation and measurement of mutually unbiased bases for time-bin qudits. Appl. Phys. Lett. *112*, 111102. https://doi.org/10.1063/1.5024318.

174. Ekert, A.K. (1991). Quantum cryptography based on Bell's theorem. Phys. Rev. Lett. *67*, 661–663. https://doi.org/10.1103/PhysRevLett.67.661.

175. Tittel, W., Brendel, J., Zbinden, H., and Gisin, N. (1998). Violation of Bell inequalities by photons more than 10 km apart. Phys. Rev. Lett. *81*, 3563–3566. https://doi.org/10.1103/PhysRevLett.81.3563.

176. Marcikic, I., De Riedmatten, H., Tittel, W., Zbinden, H., Legré, M., and Gisin, N. (2004). Distribution of time-bin entangled qubits over 50 km of optical fiber. Phys. Rev. Lett. *93*, 180502. https://doi.org/10.1103/PhysRevLett.93.180502.

177. Xu, F., Ma, X., Zhang, Q., Lo, H.K., and Pan, J.W. (2020). Secure quantum key distribution with realistic devices. Rev. Mod. Phys. *92*, 025002. https://doi.org/10.1103/RevModPhys.92.025002.

178. Weiner, A.M. (2000). Femtosecond pulse shaping using spatial light modulators. Rev. Sci. Instrum. *71*, 1929–1960. https://doi.org/10.1063/1.1150614.

179. Law, C.K., Walmsley, I.A., and Eberly, J.H. (2000). Continuous frequency entanglement: Effective finite Hilbert space and entropy control. Phys. Rev. Lett. *84*, 5304–5307. https://doi.org/10.1103/PhysRevLett.84.5304.

180. Christ, A., Laiho, K., Eckstein, A., Cassemiro, K.N., and Silberhorn, C. (2011). Probing multimode squeezing with correlation functions. New J. Phys. *13*, 033027. https://doi.org/10.1088/1367-2630/13/3/033027.

181. Liscidini, M., and Sipe, J.E. (2019). Scalable and efficient source of entangled frequency bins. Opt. Lett. *44*, 2625. https://doi.org/10.1364/OL.44.002625.

182. Wang, C., Zhang, M., Chen, X., Bertrand, M., Shams-Ansari, A., Chandrasekhar, S., Winzer, P., and Lončar, M. (2018). Integrated lithium niobate electro-optic modulators operating at CMOS-compatible voltages. Nature *562*, 101–104. https://doi.org/10.1038/s41586-018-0551-y.

183. Kharel, P., Reimer, C., Luke, K., He, L., and Zhang, M. (2021). Breaking voltage-bandwidth limits in integrated lithium niobate modulators using micro-structured electrodes. Optica *8*, 357. https://doi.org/10.1364/OPTICA.416155.

184. Lu, H.-H., Peters, N.A., Weiner, A.M., and Lukens, J.M. (2023). Characterization of quantum frequency processors. IEEE J. Sel. Top. Quant. Electron. *29*, 1–12. https://doi.org/10.1109/JSTQE.2023.3266662.

185. Lu, H.-H., Liscidini, M., Gaeta, A.L., Weiner, A.M., and Lukens, J.M. (2023). Frequency-bin photonic quantum information. Optica *10*, 1655. https://doi.org/10.1364/OPTICA.506096.

186. Barreiro, J.T., Langford, N.K., Peters, N.A., and Kwiat, P.G. (2005). Generation of hyperentangled photon pairs. Phys. Rev. Lett. *95*, 260501. https://doi.org/10.1103/PhysRevLett.95.260501.

187. Erhard, M., Malik, M., Krenn, M., and Zeilinger, A. (2018). Experimental Greenberger-Horne-Zeilinger entanglement beyond qubits. Nat. Photonics *12*, 759–764. https://doi.org/10.1038/s41566-018-0257-6.

188. Einstein, A., Podolsky, B., and Rosen, N. (1935). Can quantum-mechanical description of physical reality be considered complete? Phys. Rev. *47*, 777–780. https://doi.org/10.1103/PhysRev.47.777.

189. Mermin, N.D. (1990). Extreme quantum entanglement in a superposition of macroscopically distinct states. Phys. Rev. Lett. *65*, 1838–1840. https://doi.org/10.1103/PhysRevLett.65.1838.

190. O'Brien, J.L., Pryde, G.J., White, A.G., Ralph, T.C., and Branning, D. (2003). Demonstration of an all-optical quantum controlled-NOT gate. Nature *426*, 264–267. https://doi.org/10.1038/nature02054.

191. Fiorentino, M., and Wong, F.N.C. (2004). Deterministic controlled-NOT gate for single-photon two-qubit quantum logic. Phys. Rev. Lett. *93*, 070502. https://doi.org/10.1103/PhysRevLett.93.070502.

192. Fiorentino, M., Kim, T., and Wong, F.N.C. (2005). Single-photon two-qubit SWAP gate for entanglement manipulation. Phys. Rev. *72*, 012318. https://doi.org/10.1103/PhysRevA.72.012318.

193. Politi, A., Cryan, M.J., Rarity, J.G., Yu, S., and O'Brien, J.L. (2008). Silica-on-silicon waveguide quantum circuits. Science *320*, 646–649. https://doi.org/10.1126/science.1155441.

194. Carolan, J., Harrold, C., Sparrow, C., Martín-López, E., Russell, N.J., Silverstone, J.W., Shadbolt, P.J., Matsuda, N., Oguma, M., Itoh, M., et al. (2015). Universal linear optics. Science *349*, 711–716. https://doi.org/10.1126/science.aab3642.

195. Cheng, X., Chang, K.-C., Xie, Z., Sarihan, M.C., Lee, Y.S., Li, Y., Xu, X., Vinod, A.K., Kocaman, S., Yu, M., et al. (2023). A chip-scale polarization-spatial-momentum quantum SWAP gate in silicon nanophotonics. Nat. Photonics *17*, 656–665. https://doi.org/10.1038/s41566-023-01224-x.

196. Williams, B.P., Sadlier, R.J., and Humble, T.S. (2017). Superdense coding over optical fiber links with complete Bell-state measurements. Phys. Rev. Lett. *118*, 050501. https://doi.org/10.1103/PhysRevLett.118.050501.

197. Steinlechner, F., Ecker, S., Fink, M., Liu, B., Bavaresco, J., Huber, M., Scheidl, T., and Ursin, R. (2017). Distribution of high-dimensional entanglement via an intra-city free-space link. Nat. Commun. *8*, 15971. https://doi.org/10.1038/ncomms15971.

198. Vergyris, P., Mazeas, F., Gouzien, E., Labonté, L., Alibart, O., Tanzilli, S., and Kaiser, F. (2019). Fibre based hyperentanglement generation for dense wavelength division multiplexing. Quantum Sci. Technol. *4*, 045007. https://doi.org/10.1088/2058-9565/ab3f59.

199. Tiranov, A., Lavoie, J., Ferrier, A., Goldner, P., Verma, V.B., Nam, S.W., Mirin, R.P., Lita, A.E., Marsili, F., Herrmann, H., et al. (2015). Storage of hyperentanglement in a solid-state quantum memory. Optica *2*, 279. https://doi.org/10.1364/OPTICA.2.000279.

200. Chapman, J.C., Graham, T.M., Zeitler, C.K., Bernstein, H.J., and Kwiat, P.G. (2020). Time-bin and polarization superdense teleportation for space applications. Phys. Rev. Appl. *14*, 014044. https://doi.org/10.1103/PhysRevApplied.14.014044.

201. Lloyd, S., Shapiro, J.H., and Wong, F.N.C. (2002). Quantum magic bullets by means of entanglement. J. Opt. Soc. Am. B. *19*, 312. https://doi.org/10.1364/JOSAB.19.000312.

202. Wang, H., Horikiri, T., and Kobayashi, T. (2004). Polarization-entangled mode-locked photons from cavity-enhanced spontaneous parametric down-conversion. Phys. Rev. *70*, 043804. https://doi.org/10.1103/PhysRevA.70.043804.

203. Kuklewicz, C.E., Wong, F.N.C., and Shapiro, J.H. (2006). Time-bin-modulated biphotons from cavity-enhanced down-conversion. Phys. Rev. Lett. *97*, 223601. https://doi.org/10.1103/PhysRevLett.97.223601.

204. Wolfgramm, F., de Icaza Astiz, Y.A., Beduini, F.A., Cerè, A., and Mitchell, M.W. (2011). Atom-resonant heralded single photons by interaction-free measurement. Phys. Rev. Lett. *106*, 053602. https://doi.org/10.1103/PhysRevLett.106.053602.

205. Fekete, J., Rieländer, D., Cristiani, M., and de Riedmatten, H. (2013). Ultranarrow-band photon-pair source compatible with solid-state quantum memories and telecommunication networks. Phys. Rev. Lett. *110*, 220502. https://doi.org/10.1103/PhysRevLett.110.220502.

206. Rieländer, D., Kutluer, K., Ledingham, P.M., Gündoğan, M., Fekete, J., Mazzera, M., and De Riedmatten, H. (2014). Quantum storage of heralded single photons in a praseodymium-doped crystal. Phys. Rev. Lett. *112*, 040504. https://doi.org/10.1103/PhysRevLett.112.040504.

207. Seri, A., Lenhard, A., Rieländer, D., Gündoğan, M., Ledingham, P.M., Mazzera, M., and De Riedmatten, H. (2017). Quantum correlations between single telecom photons and a multimode on-demand solid-state quantum memory. Phys. Rev. X *7*, 021028. https://doi.org/10.1103/PhysRevX.7.021028.

208. Seri, A., Corrielli, G., Lago-Rivera, D., Lenhard, A., de Riedmatten, H., Osellame, R., and Mazzera, M. (2018). Laser-written integrated platform for quantum storage of heralded single photons. Optica *5*, 934. https://doi.org/10.1364/OPTICA.5.000934.

209. Seri, A., Lago-Rivera, D., Lenhard, A., Corrielli, G., Osellame, R., Mazzera, M., and de Riedmatten, H. (2019). Quantum storage of frequency-multiplexed heralded single photons. Phys. Rev. Lett. *123*, 080502. https://doi.org/10.1103/PhysRevLett.123.080502.

210. Lago-Rivera, D., Grandi, S., Rakonjac, J.V., Seri, A., and de Riedmatten, H. (2021). Telecom-heralded entanglement between multimode solid-state quantum memories. Nature *594*, 37–40. https://doi.org/10.1038/s41586-021-03481-8.

211. Shapiro, J.H., Kuklewicz, C.E., and Wong, F.N.C. (2004). Quantum signatures from singly-resonant and doubly-resonant parametric amplifiers. In Nonlinear Optics: Materials, Fundamentals and Applications (Optical Society of America), p. TuA5. https://doi.org/10.1364/NLO.2004.TuA5.

212. Slattery, O., Ma, L., Zong, K., and Tang, X. (2019). Background and review of cavity-enhanced spontaneous parametric down-conversion. J. Res. Natl. Inst. Stand. Technol. *124*, 1–18. https://doi.org/10.6028/jres.124.019.

213. Sangouard, N., Simon, C., De Riedmatten, H., and Gisin, N. (2011). Quantum repeaters based on atomic ensembles and linear optics. Rev. Mod. Phys. *83*, 33–80. https://doi.org/10.1103/RevModPhys.83.33.

214. Rambach, M., Nikolova, A., Weinhold, T.J., and White, A.G. (2016). Sub-megahertz linewidth single photon source. APL Photon *1*, 096101. https://doi.org/10.1063/1.4966915.

215. Müller, C., Ahlrichs, A., and Benson, O. (2020). General and complete description of temporal photon correlations in cavity-enhanced spontaneous parametric down-conversion. Phys. Rev. *102*, 053504. https://doi.org/10.1103/PhysRevA.102.053504.

216. Scholz, M., Wolfgramm, F., Herzog, U., and Benson, O. (2007). Narrow-band single photons from a single-resonant optical parametric oscillator far below threshold. Appl. Phys. Lett. *91*, 191104. https://doi.org/10.1063/1.2803761.

217. Lenhard, A., Bock, M., Becher, C., Kucera, S., Brito, J., Eich, P., Müller, P., and Eschner, J. (2015). Telecom-heralded single-photon absorption

by a single atom. Phys. Rev. *92*, 063827. https://doi.org/10.1103/PhysRevA.92.063827.

218. Pomarico, E., Sanguinetti, B., Gisin, N., Thew, R., Zbinden, H., Schreiber, G., Thomas, A., and Sohler, W. (2009). Waveguide-based OPO source of entangled photon pairs. New J. Phys. *11*, 113042. https://doi.org/10.1088/1367-2630/11/11/113042.
219. Ahlrichs, A., and Benson, O. (2016). Bright source of indistinguishable photons based on cavity-enhanced parametric down-conversion utilizing the cluster effect. Appl. Phys. Lett. *108*, 021111. https://doi.org/10.1063/1.4939925.
220. Chuu, C.S., Yin, G.Y., and Harris, S.E. (2012). A miniature ultrabright source of temporally long, narrowband biphotons. Appl. Phys. Lett. *101*, 051108. https://doi.org/10.1063/1.4740270.
221. Rieländer, D., Lenhard, A., Mazzera, M., and Riedmatten, H.d. (2016). Cavity enhanced telecom heralded single photons for spin-wave solid state quantum memories. New J. Phys. *18*, 123013. https://doi.org/10.1088/1367-2630/aa4f38.
222. Tsai, P.J., and Chen, Y.C. (2018). Ultrabright, narrow-band photon-pair source for atomic quantum memories. Quantum Sci. Technol. *3*, 034005. https://doi.org/10.1088/2058-9565/aa86e7.
223. Moqanaki, A., Massa, F., and Walther, P. (2019). Novel single-mode narrow-band photon source of high brightness tuned to cesium D2 line. APL Photon *4*, 090804. https://doi.org/10.1063/1.5095616.
224. Kumar, R., Ong, J.R., Savanier, M., and Mookherjea, S. (2014). Controlling the spectrum of photons generated on a silicon nanophotonic chip. Nat. Commun. *5*, 5489. https://doi.org/10.1038/ncomms6489.
225. Kumar, R., Savanier, M., Ong, J.R., and Mookherjea, S. (2015). Entanglement measurement of a coupled silicon microring photon pair source. Opt. Express *23*, 19318–19327. https://doi.org/10.1364/OE.23.019318.
226. Saglamyurek, E., Sinclair, N., Jin, J., Slater, J.A., Oblak, D., Bussières, F., George, M., Ricken, R., Sohler, W., and Tittel, W. (2011). Broadband waveguide quantum memory for entangled photons. Nature *469*, 512–515. https://doi.org/10.1038/nature09719.
227. Clausen, C., Usmani, I., Bussières, F., Sangouard, N., Afzelius, M., De Riedmatten, H., and Gisin, N. (2011). Quantum storage of photonic entanglement in a crystal. Nature *469*, 508–511. https://doi.org/10.1038/nature09662.
228. Saglamyurek, E., Jin, J., Verma, V.B., Shaw, M.D., Marsili, F., Nam, S.W., Oblak, D., and Tittel, W. (2015). Quantum storage of entangled telecom-wavelength photons in an erbium-doped optical fibre. Nat. Photonics *9*, 83–87. https://doi.org/10.1038/nphoton.2014.311.
229. Kim, T., Fiorentino, M., and Wong, F.N.C. (2006). Phase-stable source of polarization-entangled photons using a polarization Sagnac interferometer. Phys. Rev. *73*, 012316. https://doi.org/10.1103/PhysRevA.73.012316.
230. Kuzucu, O., and Wong, F.N.C. (2008). Pulsed Sagnac source of narrow-band polarization-entangled photons. Phys. Rev. *77*, 032314. https://doi.org/10.1103/PhysRevA.77.032314.
231. Honjo, T., Takesue, H., Kamada, H., Nishida, Y., Tadanaga, O., Asobe, M., and Inoue, K. (2007). Long-distance distribution of time-bin entangled photon pairs over 100 km using frequency up-conversion detectors. Opt. Express *15*, 13957–13964. https://doi.org/10.1364/OE.15.013957.
232. Dynes, J.F., Takesue, H., Yuan, Z.L., Sharpe, A.W., Harada, K., Honjo, T., Kamada, H., Tadanaga, O., Nishida, Y., Asobe, M., and Shields, A.J. (2009). Efficient entanglement distribution over 200 kilometers. Opt. Express *17*, 11440–11449. https://doi.org/10.1364/OE.17.011440.
233. Inagaki, T., Matsuda, N., Tadanaga, O., Asobe, M., and Takesue, H. (2013). Entanglement distribution over 300 km of fiber. Opt. Express *21*, 23241–23249. https://doi.org/10.1364/OE.21.023241.
234. Toliver, P., Dailey, J.M., Agarwal, A., and Peters, N.A. (2015). Continuously active interferometer stabilization and control for time-bin entanglement distribution. Opt. Express *23*, 4135–4143. https://doi.org/10.1364/OE.23.004135.
235. Ikuta, T., and Takesue, H. (2018). Four-dimensional entanglement distribution over 100 km. Sci. Rep. *8*, 817. https://doi.org/10.1038/s41598-017-19078-z.
236. Takesue, H., Harada, K.I., Tamaki, K., Fukuda, H., Tsuchizawa, T., Watanabe, T., Yamada, K., and Itabashi, S.I. (2010). Long-distance entanglement-based quantum key distribution experiment using practical detectors. Opt. Express *18*, 16777–16787. https://doi.org/10.1364/OE.18.016777.
237. Niu, M.Y., Xu, F., Shapiro, J.H., and Furrer, F. (2016). Finite-key analysis for time-energy high-dimensional quantum key distribution. Phys. Rev. *94*, 052323. https://doi.org/10.1103/PhysRevA.94.052323.
238. Jin, J., Bourgoin, J.P., Tannous, R., Agne, S., Pugh, C.J., Kuntz, K.B., Higgins, B.L., and Jennewein, T. (2019). Genuine time-bin-encoded quantum key distribution over a turbulent depolarizing free-space channel. Opt. Express *27*, 37214–37223. https://doi.org/10.1364/OE.27.037214.
239. Franson, J.D. (1992). Non-local cancellation of dispersion. Phys. Rev. *45*, 3126–3132. https://doi.org/10.1103/PhysRevA.45.3126.
240. Franson, J.D. (2009). Nonclassical nature of dispersion cancellation and non-local interferometry. Phys. Rev. *80*, 032119. https://doi.org/10.1103/PhysRevA.80.032119.
241. Chang, K.-C., Sarihan, M.C., Cheng, X., Zhang, Z., and Wong, C.W. (2024). Large-alphabet time-bin quantum key distribution and Einstein-Podolsky-Rosen steering via dispersive optics. Quantum Sci. Technol. *9*, 015018. https://doi.org/10.1088/2058-9565/ad0f6f.
242. Liu, X., Yao, X., Xue, R., Wang, H., Li, H., Wang, Z., You, L., Feng, X., Liu, F., Cui, K., et al. (2020). An entanglement-based quantum network based on symmetric dispersive optics quantum key distribution. APL Photon *5*, 076104. https://doi.org/10.1063/5.0002595.
243. Aktas, D., Fedrici, B., Kaiser, F., Lunghi, T., Labonté, L., and Tanzilli, S. (2016). Entanglement distribution over 150 km in wavelength division multiplexed channels for quantum cryptography. Laser Photon. Rev. *10*, 451–457. https://doi.org/10.1002/lpor.201500258.
244. Wengerowsky, S., Joshi, S.K., Steinlechner, F., Hübel, H., and Ursin, R. (2018). An entanglement-based wavelength-multiplexed quantum communication network. Nature *564*, 225–228. https://doi.org/10.1038/s41586-018-0766-y.
245. Joshi, S.K., Aktas, D., Wengerowsky, S., Lončarić, M., Neumann, S.P., Liu, B., Scheidl, T., Lorenzo, G.C., Samec, Ž., Kling, L., et al. (2020). A trusted node-free eight-user metropolitan quantum communication network. Sci. Adv. *6*, eaba0959. https://doi.org/10.1126/sciadv.aba0959.
246. Kim, J.-H., Chae, J.-W., Jeong, Y.-C., and Kim, Y.-H. (2022). Quantum communication with time-bin entanglement over a wavelength-multiplexed fiber network. APL Photon *7*, 016106. https://doi.org/10.1063/5.0073040.
247. Fujimoto, R., Yamazaki, T., Kobayashi, T., Miki, S., China, F., Terai, H., Ikuta, R., and Yamamoto, T. (2022). Entanglement distribution using a biphoton frequency comb compatible with DWDM technology. Opt. Express *30*, 36711–36716. https://doi.org/10.1364/OE.469344.
248. Wen, W., Chen, Z., Lu, L., Yan, W., Xue, W., Zhang, P., Lu, Y., Zhu, S., and Ma, X.S. (2022). Realizing an entanglement-based multiuser quantum network with integrated photonics. Phys. Rev. Appl. *18*, 024059. https://doi.org/10.1103/PhysRevApplied.18.024059.
249. Niizeki, K., Yoshida, D., Ito, K., Nakamura, I., Takei, N., Okamura, K., Zheng, M.Y., Xie, X.P., and Horikiri, T. (2020). Two-photon comb with wavelength conversion and 20-km distribution for quantum communication. Commun. Phys. *3*, 138. https://doi.org/10.1038/s42005-020-00406-1.
250. Bourennane, M., Karlsson, A., and Björk, G. (2001). Quantum key distribution using multilevel encoding. Phys. Rev. *64*, 012306. https://doi.org/10.1103/PhysRevA.64.012306.

251. Cozzolino, D., Da Lio, B., Bacco, D., and Oxenløwe, L.K. (2019). High-Dimensional Quantum Communication: Benefits, Progress, and Future Challenges. Adv. Quantum Technol. *2*, 1900038. https://doi.org/10.1002/qute.201900038.

252. Pirandola, S., Andersen, U.L., Banchi, L., Berta, M., Bunandar, D., Colbeck, R., Englund, D., Gehring, T., Lupo, C., Ottaviani, C., et al. (2020). Advances in quantum cryptography. Adv. Opt Photon *12*, 1012. https://doi.org/10.1364/AOP.361502.

253. Paraïso, T.K., Woodward, R.I., Marangon, D.G., Lovic, V., Yuan, Z., and Shields, A.J. (2021). Advanced Laser Technology for Quantum Communications (Tutorial Review). Adv. Quan. Technol. *4*, 2100062. https://doi.org/10.1002/qute.202100062.

254. Bouchard, F., England, D., Bustard, P.J., Fenwick, K.L., Karimi, E., Heshami, K., and Sussman, B. (2021). Achieving ultimate noise tolerance in quantum communication. Phys. Rev. Appl. *15*, 024027. https://doi.org/10.1103/PhysRevApplied.15.024027.

255. Jiang, M.H., Xue, W., He, Q., An, Y.Y., Zheng, X., Xu, W.J., Xie, Y.B., Lu, Y., Zhu, S., and Ma, X.S. (2023). Quantum storage of entangled photons at telecom wavelengths in a crystal. Nat. Commun. *14*, 6995. https://doi.org/10.1038/s41467-023-42741-1.

256. Liao, S.-K., Cai, W.-Q., Liu, W.-Y., Zhang, L., Li, Y., Ren, J.-G., Yin, J., Shen, Q., Cao, Y., Li, Z.-P., et al. (2017). Satellite-to-ground quantum key distribution. Nature *549*, 43–47. https://doi.org/10.1038/nature23655.

257. Liao, S.-K., Cai, W.-Q., Handsteiner, J., Liu, B., Yin, J., Zhang, L., Rauch, D., Fink, M., Ren, J.-G., Liu, W.-Y., et al. (2018). Satellite-relayed intercontinental quantum network. Phys. Rev. Lett. *120*, 030501. https://doi.org/10.1103/PhysRevLett.120.030501.

258. Yin, J., Li, Y.-H., Liao, S.-K., Yang, M., Cao, Y., Zhang, L., Ren, J.-G., Cai, W.Q., Liu, W.-Y., Li, S.-L., et al. (2020). Entanglement-based secure quantum cryptography over 1,120 kilometres. Nature *582*, 501–505. https://doi.org/10.1038/s41586-020-2401-y.

259. Chen, Y.-A., Zhang, Q., Chen, T.-Y., Cai, W.-Q., Liao, S.-K., Zhang, J., Chen, K., Yin, J., Ren, J.-G., Chen, Z., et al. (2021). An integrated space-to-ground quantum communication network over 4,600 kilometres. Nature *589*, 214–219. https://doi.org/10.1038/s41586-020-03093-8.

260. Muthukrishnan, A., and Stroud, C.R. (2000). Multivalued logic gates for quantum computation. Phys. Rev. *62*, 052309. https://doi.org/10.1103/PhysRevA.62.052309.

261. Luo, M., and Wang, X. (2014). Universal quantum computation with qudits. Sci. China Phys. Mech. Astron. *57*, 1712–1717.

262. Javid, U.A., Lopez-Rios, R., Ling, J., Graf, A., Staffa, J., and Lin, Q. (2023). Chip-scale simulations in a quantum-correlated synthetic space. Nat. Photonics *17*, 883–890. https://doi.org/10.1038/s41566-023-01236-7.

263. Kaszlikowski, D., Gnaciński, P., Żukowski, M., Miklaszewski, W., and Zeilinger, A. (2000). Violations of local realism by two entangled N-dimensional systems are stronger than for two qubits. Phys. Rev. Lett. *85*, 4418–4421. https://doi.org/10.1103/PhysRevLett.85.4418.

264. Wang, X.-L., Chen, L.-K., Li, W., Huang, H.-L., Liu, C., Chen, C., Luo, Y.-H., Su, Z.-E., Wu, D., Li, Z.-D., et al. (2016). Experimental ten-photon entanglement. Phys. Rev. Lett. *117*, 210502. https://doi.org/10.1103/PhysRevLett.117.210502.

265. Bullock, S.S., O'Leary, D.P., and Brennen, G.K. (2005). Asymptotically optimal quantum circuits for *d*-level systems. Phys. Rev. Lett. *94*, 230502. https://doi.org/10.1103/PhysRevLett.94.230502.

266. Niu, M.Y., Chuang, I.L., and Shapiro, J.H. (2018). Qudit-basis universal quantum computation using $\chi^{(2)}$ interactions. Phys. Rev. Lett. *120*, 160502. https://doi.org/10.1103/PhysRevLett.120.160502.

267. Alexander, R.N., Wang, P., Sridhar, N., Chen, M., Pfister, O., and Menicucci, N.C. (2016). One-way quantum computing with arbitrarily large time-frequency continuous-variable cluster states from a single optical parametric oscillator. Phys. Rev. *94*, 032327. https://doi.org/10.1103/PhysRevA.94.032327.

268. Sciara, S., Reimer, C., Kues, M., Roztocki, P., Cino, A., Moss, D.J., Caspani, L., Munro, W.J., and Morandotti, R. (2019). Universal *N*-Partite *d*-Level Pure-State Entanglement Witness Based on Realistic Measurement Settings. Phys. Rev. Lett. *122*, 120501. https://doi.org/10.1103/PhysRevLett.122.120501.

269. Roztocki, P., Sciara, S., Reimer, C., Cortés, L.R., Zhang, Y., Wetzel, B., Islam, M., Romero Cortés, L., Cino, A., Chu, S.T., et al. (2019). Complex quantum state generation and coherent control based on integrated frequency combs. J. Lightwave Technol. *37*, 338–344. https://doi.org/10.1109/JLT.2018.2880934.

270. Sciara, S., Roztocki, P., Fischer, B., Reimer, C., Romero Cortés, L., Munro, W.J., Moss, D.J., Cino, A.C., Caspani, L., Kues, M., et al. (2021). Scalable and effective multi-level entangled photon states: A promising tool to boost quantum technologies. Nanophotonics *10*, 4447–4465. https://doi.org/10.1515/nanoph-2021-0510.

271. Roztocki, P., Kues, M., Reimer, C., Wetzel, B., Sciara, S., Zhang, Y., Cino, A., Little, B.E., Chu, S.T., Moss, D.J., and Morandotti, R. (2017). Practical system for the generation of pulsed quantum frequency combs. Opt. Express *25*, 18940–18949. https://doi.org/10.1364/OE.25.018940.

272. Roztocki, P., MacLellan, B., Islam, M., Reimer, C., Fischer, B., Sciara, S., Romero Cortés, L., Jestin, Y., Cino, A., Chu, S.T., et al. (2021). Arbitrary phase access for stable fiber interferometers. Laser Photon. Rev. *15*, 2000524. https://doi.org/10.1002/lpor.202000524.

273. Yamazaki, T., Arizono, T., Kobayashi, T., Ikuta, R., and Yamamoto, T. (2023). Linear optical quantum computation with frequency-comb qubits and passive devices. Phys. Rev. Lett. *130*, 200602. https://doi.org/10.1103/PhysRevLett.130.200602.

274. Briegel, H.J., and Raussendorf, R. (2001). Persistent entanglement in arrays of interacting particles. Phys. Rev. Lett. *86*, 910–913. https://doi.org/10.1103/PhysRevLett.86.910.

275. Raussendorf, R., and Briegel, H.J. (2001). A one-way quantum computer. Phys. Rev. Lett. *86*, 5188–5191. https://doi.org/10.1103/PhysRevLett.86.5188.

276. Nielsen, M.A. (2004). Optical quantum computation using cluster states. Phys. Rev. Lett. *93*, 040503. https://doi.org/10.1103/PhysRevLett.93.040503.

277. Wang, Y., Hu, Z., Sanders, B.C., and Kais, S. (2020). Qudits and high-dimensional quantum computing. Front. Physiol. *8*, 479. https://doi.org/10.3389/fphy.2020.589504.

278. Awschalom, D., Berggren, K.K., Bernien, H., Bhave, S., Carr, L.D., Davids, P., Economou, S.E., Englund, D., Faraon, A., Fejer, M., et al. (2021). Development of quantum interconnects (quics) for next-generation information technologies. PRX Quan *2*, 017002. https://doi.org/10.1103/PRXQuantum.2.017002.

279. Kumar, P. (1990). Quantum frequency conversion. Opt. Lett. *15*, 1476–1478. https://doi.org/10.1364/OL.15.001476.

280. Xie, Z., Luo, K.H., Chang, K.-C., Panoiu, N.C., Herrmann, H., Silberhorn, C., and Wong, C.W. (2019). Efficient C-band single-photon upconversion with chip-scale Ti-indiffused pp-LiNbO3 waveguides. Appl. Opt. *58*, 5910–5915. https://doi.org/10.1364/AO.58.005910.

281. Lauk, N., Sinclair, N., Barzanjeh, S., Covey, J.P., Saffman, M., Spiropulu, M., and Simon, C. (2020). Perspectives on quantum transduction. Quantum Sci. Technol. *5*, 020501. https://doi.org/10.1088/2058-9565/ab788a.

282. Sanaka, K., Kawahara, K., and Kuga, T. (2002). Experimental probabilistic manipulation of down-converted photon pairs using unbalanced interferometers. Phys. Rev. *66*, 040301. https://doi.org/10.1103/PhysRevA.66.040301.

283. Donohue, J.M., Agnew, M., Lavoie, J., and Resch, K.J. (2013). Coherent ultrafast measurement of time-bin encoded photons. Phys. Rev. Lett. *111*, 153602. https://doi.org/10.1103/PhysRevLett.111.153602.

284. Fickler, R., Lapkiewicz, R., Huber, M., Lavery, M.P.J., Padgett, M.J., and Zeilinger, A. (2014). Interface between path and orbital angular momentum entanglement for high-dimensional photonic quantum information. Nat. Commun. *5*, 4502. https://doi.org/10.1038/ncomms5502.

285. Kupchak, C., Bustard, P.J., Heshami, K., Erskine, J., Spanner, M., England, D.G., and Sussman, B.J. (2017). Time-bin-to-polarization conversion of ultrafast photonic qubits. Phys. Rev. *96*, 053812. https://doi.org/10.1103/PhysRevA.96.053812.

286. Degen, C.L., Reinhard, F., and Cappellaro, P. (2017). Quantum sensing. Rev. Mod. Phys. *89*, 035002. https://doi.org/10.1103/RevModPhys.89.035002.

287. Altman, E., Brown, K.R., Carleo, G., Carr, L.D., Demler, E., Chin, C., DeMarco, B., Economou, S.E., Eriksson, M.A., Fu, K.-M.C., et al. (2021). Quantum simulators: Architectures and opportunities. PRX Quan. *2*, 017003. https://doi.org/10.1103/PRXQuantum.2.017003.

288. Alexeev, Y., Bacon, D., Brown, K.R., Calderbank, R., Carr, L.D., Chong, F.T., DeMarco, B., Englund, D., Farhi, E., Fefferman, B., et al. (2021). Quantum computer systems for scientific discovery. PRX Quan *2*, 017001. https://doi.org/10.1103/PRXQuantum.2.017001.

289. Lukens, J.M., and Lougovski, P. (2017). Frequency-encoded photonic qubits for scalable quantum information processing. Optica *4*, 8. https://doi.org/10.1364/OPTICA.4.000008.

290. Seshadri, S., Lu, H.H., Leaird, D.E., Weiner, A.M., and Lukens, J.M. (2022). Complete frequency-bin Bell basis synthesizer. Phys. Rev. Lett. *129*, 230505. https://doi.org/10.1103/PhysRevLett.129.230505.